Double Exchange and Vibronic Coupling in Mixed-Valence Systems. Electronic Structure of Exchange-Coupled Siroheme−$[Fe_4S_4]^{2+}$ Chromophore in Oxidized *E. Coli* Sulfite Reductase

Emile L. Bominaar,[†] Zhengguo Hu,[†] Eckard Münck,*[,†] Jean-Jacques Girerd,[‡] and Sergueï A. Borshch[§]

Contribution from the Department of Chemistry, Carnegie-Mellon University, Pittsburgh, Pennsylvania 15213, Laboratoire de Chimie Inorganique, URA CNRS 420, Institut de Chimie Moléculaire, d'Orsay, Université de Paris-Sud, 91405 Orsay, France, and Institut de Recherches sur la Catalyse, CNRS, 69626 Villeurbanne cedex, France

Received February 21, 1995[⊗]

Abstract: The oxidized state of the active site of *E. coli* sulfite reductase (SiR^0) consists of two covalently linked chromophores, a siroheme and an $[Fe_4S_4]^{2+}$ cluster. This work is motivated by the observation of paramagnetic hyperfine structure at the ^{57}Fe sites of the $[Fe_4S_4]^{2+}$ moiety, a species which is diamagnetic if it were an isolated cluster. The first part of the paper presents the results for the ubiquitous $[Fe_4S_4]^{2+}$ core that is found in enzymes, proteins, and synthetic analogs. The core is analyzed in the framework of an effective-Hamiltonian model, including terms for itinerant electron transfer and antiferromagnetic exchange. Spin-dependent electron delocalization (double exchange) in clusters with T_d symmetry gives rise to degenerate ground states for both positive and negative transfer parameters, β_0. A vibronic coupling mechanism is introduced that is based on the structure dependence of the transfer parameters, $\beta_{ij} = \beta_0 + \Lambda\Delta r_{ij}$. The vibronic coupling leads to Jahn−Teller distortion of the $[Fe_4S_4]^{2+}$ core from T_d to D_{2d}, in agreement with the idealized symmetries observed in $[Fe_4S_4]^{2+}$ cores in proteins and synthetic analogs with thiolate terminal ligands. The broken-symmetry, D_{2d}, ground states consist of two electronically delocalized Fe pairs, (A,B) and (C,D), of maximum spin ($S_{AB} = S_{CD} = 9/2$), or nearly so, which are coupled by antiferromagnetic exchange coupling (J_{cube}) to a resultant diamagnetic state, $S_{cube} = 0$. The delocalized pairs are "locked-in" by distortion-enhanced double-exchange interactions in the two pairs. The second part of the paper is devoted to the changes induced in the spin state of the cluster by the exchange coupling, $J_H\vec{S}_D\cdot\vec{S}_H$, between one of the cubane sites (D) and an external Fe site ($S_H = 5/2$), where the latter site is representing the heme iron in SiR^0. Except for the weak vibronic coupling limit, the 5-spin coupling problem (S_X, X = A, B, C, D, H) can be cast into a 3-spin coupling problem ($S_{AB} = S_{CD} = 9/2$, S_H). The heme−cluster coupling admixes a spin triplet ($S_{cube} = 1$) into the diamagnetic ground state of the Fe−S cluster by which the cube acquires paramagnetic properties. The resulting magnetic hyperfine coupling constants at the four Fe sites of the cube have almost equal magnitude but are pairwise of opposite sign, in agreement with the results, $A^A \approx A^B \approx -A^C \approx -A^D$, deduced from analyses of the Mössbauer spectra of SiR^0. For $|J_H| \ll J_{cube}$, the ratio of the effective A^X-values and the intrinsic a-values of the iron sites can be expressed as $|A^X/a| \approx 4.1|J_H/J_{cube}|$. Using empirical estimates for $|A^X/a|$ and J_{cube}, the value for J_H is found to be about ± 17 cm^{-1}.

Introduction

Theoretical studies of mixed-valent Fe−S clusters have revealed that the combination of double exchange and vibronic interaction provides a mechanism for the interpretation of the electron delocalization patterns and spin states in systems that accommodate a single itinerant electron moving in a background of high-spin Fe^{III} cores.[1] Double exchange promotes parallel coupling of the core spins in binuclear mixed-valence systems with paramagnetic sites.[2] Jahn−Teller distortions in tri- and tetranuclear systems "lock-in" electronic states arising from double exchange, for which the major part of the itinerant-electron charge is distributed over two equivalent sites of the clusters.[1] This theoretical result is in agreement with the pair delocalization observed in Mössbauer studies of the reduced $[Fe_3S_4]^0$ cluster in *D. gigas* ferredoxin II[3] and other proteins,[4] as well as in the triiron subunits of clusters with MFe_3S_4 cores (M = Mo, W, Co, Ni, Zn)[5a−e] and M = Fe.[5f] Pair delocalization patterns have also been observed in $[Fe_4S_4]^{1+,3+}$ clusters in proteins[6,7] and synthetic analogs.[8,9] The observation of pair delocalization in chemically symmetric model complexes[5,8,9] indicates that this phenomenon is not primarily controlled by protein structure but is rather an intrinsic property of the Fe−S

[†] Carnegie-Mellon University.
[‡] Université de Paris-Sud.
[§] Institut de Recherches sur la Catalyse.
[⊗] Abstract published in *Advance ACS Abstracts*, June 15, 1995.

(1) (a) Borshch, S. A.; Chibotaru, L. F. *Chem. Phys.* **1989**, *135*, 375−380. (b) Borshch, S. A.; Bominaar, E. L.; Girerd, J.-J. *New J. Chem.* **1993**, *17*, 39−42. (c) Borshch, S. A.; Bominaar, E. L.; Blondin, G.; Girerd, J.-J. *J. Am. Chem. Soc.* **1993**, *115*, 5155−5168. (d) Bominaar, E. L.; Borshch, S. A.; Girerd, J.-J. *J. Am. Chem. Soc.* **1994**, *116*, 5362−5372.

(2) (a) Zener, C. *Phys. Rev.* **1951**, *82*, 403−405. (b) Anderson, P. W.; Hasegawa, H. *Phys. Rev.* **1955**, *100*, 675−681. (c) Ding, X.-Q.; Bominaar, E. L.; Bill, E.; Winkler, H.; Trautwein, A. X.; Drüeke, S.; Chaudhuri, P.; Wieghardt, K. *J. Chem. Phys.* **1990**, *92*, 178−186.

(3) Papaefthymiou, V.; Girerd, J.-J.; Moura, I.; Moura, J. J. G.; Münck, E. *J. Am. Chem. Soc.* **1987**, *109*, 4703−4710.

(4) (a) Surerus, K. K.; Kennedy, M. C.; Beinert, H.; Münck, E. *Proc. Natl. Acad. Sci. U.S.A.* **1989**, *86*, 9846−9850. (b) Emptage, M. H.; Kent, T. A.; Huynh, B. H.; Rawlings, J.; Orme-Johnson, W. H.; Münck, E. *J. Biol. Chem.* **1980**, *255*, 1793−1796.

0002-7863/95/1517-6976$09.00/0

clusters and suggests the application of Jahn−Teller theory to these systems.[1] Furthermore, the spin dependence of the vibronic stabilization energies gives rise to an effective spin-coupling mechanism which may already stabilize an $S = 2$ ground state in the $[Fe_3S_4]^0$ cluster, even in the absence of antiferromagnetic Heisenberg−Dirac−Van Vleck (HDVV) exchange.[1c,d]

In this study, we have extended our theoretical analysis to the two-itinerant-electron containing $[Fe_4S_4]^{2+}$ clusters. Such clusters have been synthesized[8,10−13] and are found in many proteins and enzymes.[14] $[Fe_4S_4]^{2+}$ clusters have, without exception, a diamagnetic ground state ($S_{cube} = 0$)[8,13−15] which excludes detailed studies of the spin coupling with Mössbauer spectroscopy because magnetic hyperfine interactions are absent. X-ray studies of both the proteins[16] and the synthetic model compounds[11−13] have revealed that cubanes in the +2 core-oxidation state have nearly D_{2d} symmetries with slight contraction along the S_4 symmetry axis.[10] The distributions of the two itinerant electrons over the four Fe sites, as attested by Mössbauer isomer shifts, are homogeneous, i.e. half an itinerant electron charge per site.[7b,14]

The work described below was prompted by a series of Mössbauer studies of *E. coli* sulfite reductase (SiR),[17−21] an enzyme that catalyzes the six-electron reduction of sulfite to sulfide.[22] The β subunit of this enzyme contains one siroheme and one Fe_4S_4 cluster. Quite surprisingly, the Mössbauer spectra of SiR exhibited ^{57}Fe magnetic hyperfine interactions at all iron sites of the iron−sulfur cluster even when the cluster was in the ("diamagnetic") 2+ oxidation state. These observations were explained by postulating a superexchange pathway linking the heme iron with one iron site of the Fe_4S_4 cluster, implying that the cluster and the siroheme are covalently bridged by a ligand. Superexchange between the paramagnetic heme and the iron sulfur cluster can mix paramagnetic excited states of the $[Fe_4S_4]^{2+}$ cluster into its ground state such that the latter acquires paramagnetic properties as witnessed by the observation of magnetic hyperfine structure in the Mössbauer spectra.[21] More recently, the structural link between the siroheme and the $[Fe_4S_4]^{2+}$ cluster was explicitly formulated[23a] as a cysteinyl sulfur atom based on X-ray data[23b] and the spectroscopic results (see below).

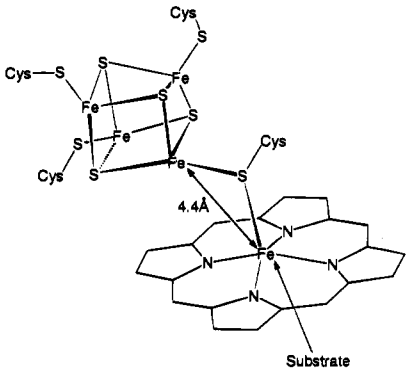

SiR can be studied in a variety of oxidation and complexation states. The heme can be ferric or ferrous while the cluster can be in either the 2+ or the 1+ core oxidation state. Moreover, the heme can bind ligands such as CO, CN^-, SO_3^{2-}, NO_2^-, S^{2-}, and NO.[24] Since the exchange pathway between the heme iron and the cluster is maintained in all oxidation and complexation states studied,[20] we may assume that these ligands bind to the sixth coordination site of the heme. The uncomplexed enzyme has three stable oxidation states, labeled SiR^0 for the oxidized (as isolated) enzyme, and SiR^{1-} and SiR^{2-} for the 1-electron and 2-electron reduced protein, respectively. In SiR^{1-} the heme iron is ferrous (probably intermediate spin $S_H = 1$[17,18,20]) while the cluster remains in the same (2+) state as in the oxidized enzyme. SiR^{2-} comprises a high-spin ferrous heme and $[Fe_4S_4]^{1+}$.[19]

In SiR^0 and SiR^{1-}, the four iron sites of the $[Fe_4S_4]^{2+}$ cluster have the same temperature-independent quadrupole splitting, $\Delta E_Q = 1.0$ mm/s, and isomer shift, $\delta = 0.45$ mm/s (at 4.2 K). The value of δ, the visible spectra, and the redox behavior unambiguously identify the 2+ oxidation state of the cluster,

(5) (a) Moura, I.; Moura, J. J. G.; Münck, E.; Papaefthymiou, V.; LeGall, J. *J. Am. Chem. Soc.* **1986**, *108*, 349−351. (b) Coucouvanis, D.; Al-Ahmad, S. A.; Salifoglou, A.; Papaefthymiou, V.; Kostikas, A.; Simopoulos, A. *J. Am. Chem. Soc.* **1992**, *114*, 2472−2482. (c) Srivastava, K. K. P.; Surerus, K. K.; Conover, R. C.; Johnson, M. K.; Park, J. B.; Adams, M. W. W.; Münck, E. *Inorg. Chem.* **1993**, *32*, 927−936. (d) Zhou, J.; Scott, M. J.; Hu, Z.; Peng, G.; Münck, E.; Holm, R. H. *J. Am. Chem. Soc.* **1992**, *114*, 10843−10854. (e) Surerus, K. K.; Münck, E.; Moura, I.; Moura, J. J. G.; LeGall, J. *J. Am. Chem. Soc.* **1987**, *109*, 3805−3807. (f) Weigel, J. A.; Srivastava, K. K. P.; Day, E. P.; Münck, E.; Holm, R. H. *J. Am. Chem. Soc.* **1990**, *112*, 8015−8023.

(6) Middleton, P.; Dickson, D. P. E.; Johnson, C. E.; Rush, J. D. *Eur. J. Biochem.* **1978**, *88*, 135−141.

(7) (a) Dickson, D. P. E.; Johnson, C. E.; Cammack, R.; Evans, M. C. W.; Hall, D. O.; Rao, K. K. *Biochem. J.* **1974**, *139*, 105−108. (b) Middleton, P.; Dickson, D. P. E.; Johnson, C. E.; Rush, J. D. *Eur. J. Biochem.* **1980**, *104*, 289−296. (c) Münck, E.; Papaefthymiou, V.; Surerus, K. K.; Girerd, J.-J. In *Metal Ions in Proteins*; Que, L., Ed.; ACS Symp. Ser. 372; American Chemical Society: Washington, DC, 1988; Chapter 15, pp 302−325.

(8) Laskowski, E. J.; Frankel, R. B.; Gillum, W. O.; Papaefthymiou, G. C.; Renaud, J.; Ibers, J. A.; Holm, R. H. *J. Am. Chem. Soc.* **1978**, *100*, 5322−5337.

(9) Papaefthymiou, V.; Millar, M. M.; Münck, E. *Inorg. Chem.* **1986**, *25*, 3010−3014.

(10) Berg, J. M.; Holm, R. H. In *Metal Ions in Biology*; Spiro, T. G., Ed.; Interscience: New York, 1982; Vol. 4, Chapter 1, pp 1−66.

(11) Herskovitz, T.; Averill, B. A.; Holm, R. H.; Ibers, J. A.; Phillips, W. D.; Weiher, J. F. *Proc. Natl. Acad. Sci. U.S.A.* **1972**, *69*, 2437−2441.

(12) (a) Averill, B. A.; Herskovitz, T.; Holm, R. H.; Ibers, J. A. *J. Am. Chem. Soc.* **1973**, *95*, 3523−3534. (b) Bobrik, M. A.; Hodgson, K. O.; Holm, R. H. *Inorg. Chem.* **1977**, *16*, 1851−1858. (c) Que, L.; Bobrik, M. A.; Ibers, J. A.; Holm, R. H. *J. Am. Chem. Soc.* **1974**, *96*, 4168−4178. (d) Laskowski, E. J.; Reynolds, J. G.; Frankel, R. B.; Foner, S.; Papaefthymiou, G.C.; Holm, R. H. *J. Am. Chem. Soc.* **1979**, *101*, 6562−6570.

(13) (a) Wong, G. B.; Bobrik, M. A.; Holm, R. H. *Inorg. Chem.* **1978**, *17*, 578−584. (b) Cleland, W. E.; Holtman, D. A.; Sabat, M.; Ibers, J. A.; DeFotis, G. C.; Averill, B. A. *J. Am. Chem. Soc.* **1983**, *105*, 6021−6031.

(14) Cammack, R. In *Advances in Inorganic Chemistry*; Sykes, A. G., Ed.; Academic Press: New York, 1992; Vol. 38, pp 281−322 and references therein.

(15) (a) Moss, T. H.; Petering, D.; Palmer, G. *J. Biol. Chem.* **1969**, *244*, 2275−2277. (b) Antanaitis, B. C.; Moss, T. H. *Biochim. Biophys. Acta* **1975**, *405*, 262−279.

(16) (a) Freer, S. T.; Alden, R. A.; Carter, C. W.; Kraut, J. *J. Biol. Chem.* **1975**, *250*, 46−54. (b) Howard, J. B.; Rees, D. C. In *Advances in Protein Chemistry*; Anfinsen, C. B., Edsall, J. T., Eisenberg, D. S., Richards, F. M., Eds.; Academic Press: San Diego, 1991; Vol. 42, pp 199−280 and references therein.

(17) Christner, J. A.; Münck, E.; Janick, P. A.; Siegel, L. M. *J. Biol. Chem.* **1981**, *256*, 2098−2101.

(18) (a) Christner, J. A.; Münck, E.; Janick, P. A.; Siegel, L. M. *J. Biol. Chem.* **1983**, *258*, 11147−11156. (b) Christner, J. A.; Janick, P. A.; Siegel, L. M.; Münck, E. *J. Biol. Chem.* **1983**, *258*, 11157−11164.

(19) Christner, J. A.; Münck, E.; Kent, T. A.; Janick, P. A.; Salerno, J. C.; Siegel, L. M. *J. Am. Chem. Soc.* **1984**, *106*, 6786−6794.

(20) Christner, J. A. Ph.D. Thesis, University of Minnesota, 1983.

(21) Münck, E. In *Iron Sulfur Proteins*; Spiro, T. G., Ed.; Interscience: New York, 1982; Chapter 4, pp 147−175.

(22) Siegel, L. M. In *Mechanisms of Oxidizing Enzymes*; Singer, T. P., Ondarza, R. N., Eds.; Elsevier-North Holland: New York, 1978; pp 201−214.

(23) (a) Ostrowski, J.; Wu, J. Y.; Rueger, D. C.; Miller, B. E.; Siegel, L. M.; Kredich, N. M. *J. Biol. Chem.* **1989**, *264*, 15726−15737. (b) McRee, D. E.; Richardson, D. C.; Richardson, J. S.; Siegel, L. M. *J. Biol. Chem.* **1986**, *261*, 10277−10281.

(24) (a) Siegel, L. M.; Rueger, D. C.; Barber, M. J.; Krueger, R. J.; Orme-Johnson, N. R.; Orme-Johnson, W. H. *J. Biol. Chem.* **1982**, *257*, 6343−6350. (b) Janick, P. A.; Siegel, L. M. *Biochemistry* **1982**, *21*, 3538−3547. (c) Janick, P. A.; Siegel, L. M. *Biochemistry* **1983**, *22*, 504−515. (d) Janick, P. A.; Rueger, D. C.; Krueger, R. J.; Barber, M. J.; Siegel, L. M. *Biochemistry* **1983**, *22*, 396−408.

and the observation of the same ΔE_Q and δ at the four iron sites of the cluster suggests delocalization of the iron valencies. The observation of the same values for ΔE_Q and δ in SiR^0 and SiR^{1-} shows that the electronic (orbital) structure of the cluster is independent of the oxidation state of the heme iron. Moreover, the temperature independence of ΔE_Q indicates the absence of excited *orbital* states at energies below circa 700 cm^{-1}.

In SiR^0 the heme iron is high-spin ($S_H = 5/2$) ferric. The low-temperature Mössbauer spectrum of the siroheme was found to exhibit magnetic hyperfine interactions typical of monomeric hemes.[17] Because of the exchange coupling to the heme, the Mössbauer spectra of the iron sites of the $[Fe_4S_4]^{2+}$ cluster exhibit magnetic hyperfine interactions as well. It has been shown[17] that the temperature dependence and the response of these magnetic hyperfine interactions to an externally applied magnetic field can be described by the spin Hamiltonian $\vec{S}\cdot\sum A^X\vec{I}_X$, where X sums over the iron sites of the cluster, and the heme, where $S = 5/2$ is common to all five sites. The A-values of the $[Fe_4S_4]^{2+}$ cluster were found to occur in equivalent pairs such that $A^A \approx A^B \approx -A^C \approx -A^D$ with $|A^X| \approx$ 6.3 MHz, suggesting that the electronic structure of the cluster can be described by pairs of delocalized iron sites. The A-values obtained by Mössbauer spectroscopy were confirmed by detailed ENDOR studies of SiR^0 by B. M Hoffman and co-workers;[25] these studies, in particular, support the idea of coupled chromophores because ^{57}Fe ENDOR of the cubane iron sites is observed when the applied field is tuned to the $S = 5/2$ EPR signal.

Because the ground state of $[Fe_4S_4]^{2+}$ clusters is diamagnetic, experimental access for determining the exchange interactions is limited to magnetic susceptibility studies[8,13,15b] and ambient temperature ^1H NMR.[26] Mössbauer, EPR, and ENDOR spectroscopies which have furnished a wealth of information on exchange coupled systems having a paramagnetic ground state are thus not suitable for studies of exchange interactions in magnetically isolated $[Fe_4S_4]^{2+}$ clusters. Perturbation of the internal structure of the $[Fe_4S_4]^{2+}$ cluster in SiR^0 through coupling to the paramagnetic siroheme offers an opportunity for studying exchange interactions in the 2+ state of the cubanes. Recently, Cai and Holm[27] have succeeded in constructing heme−cube assemblies with a variety of bridging ligands; study of these systems will provide further insight into the electronic structure of the biologically very important $[Fe_4S_4]^{2+}$ core.

This paper is organized as follows. An effective Hamiltonian is introduced that includes terms for electron-transfer interaction, HDVV exchange, and vibronic coupling. The vibronic coupling mechanism considered here differs from the mechanism introduced by Piepho, Krausz, and Schatz (PKS model) in the study of binuclear mixed-valence compounds,[28] in that it makes the transfer interactions in the 2+ cluster dependent on distortions from idealized T_d symmetry. The effective Hamiltonian will first be applied to the isolated $[Fe_4S_4]^{2+}$ cluster. Just as for systems with one itinerant electron, the ground state space of the transfer operator in the 2+ cluster is highly degenerate, rendering the cluster susceptible to Jahn−Teller distortion.[1] The adiabatic potential surfaces for the $d^5-d^5-d^6-d^6$ valence state of the +2 cluster are determined and their extremal points, corresponding to definite spin states, are ascertained. This

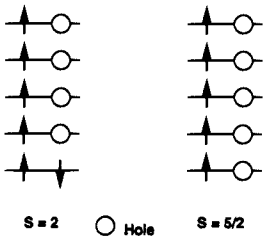

Figure 1. Relationship between electron and hole configurations in high-spin ferrous iron (left) and high-spin ferric iron (right).

treatment is followed by an analysis of the changes in the broken-symmetry ground state of the $[Fe_4S_4]^{2+}$ cluster induced by an exchange coupling between one of its Fe sites, Fe_D, and an external high-spin Fe^{III} heme, Fe_H. Special attention is paid to the magnetic hyperfine coupling constants, A^X, of the Fe sites of the $[Fe_4S_4]^{2+}$ cluster. Comparison of the A^X values with the experimental data reported for SiR^0 provides an estimate of the strength of the exchange coupling between siroheme iron and Fe_D.

Theoretical Model for $[Fe_4S_4]^{2+}$

Electronic Basis States. We consider a tetranuclear cluster of tetrahedral symmetry (T_d) with high-spin iron sites A, B, C, and D. The formal valences of the iron sites are $d^5-d^5-d^6-d^6$. There are five localized, orthogonal, Wannier-type orbitals at each center: $|a\rangle$, $|a_i\rangle$, $|b\rangle$, $|b_i\rangle$, $|c\rangle$, $|c_i\rangle$, and $|d\rangle$, $|d_i\rangle$, with $i = 1-4$. Orbital pairs like a_i and b_i and a and b are interchangeable by symmetry operation. The indexed orbitals are singly occupied while the non-indexed orbitals are singly occupied at the two ferric (d^5) sites and doubly occupied at the two ferrous (d^6) sites. The unpaired electron spins at each Fe site are coupled parallel in order to obey Hund's rule, leading to local spins $S_X = 5/2$ (ferric) and $S_X{}^0 = 2$ (ferrous), with X = A, B, C, or D. The space of electronic cluster states considered here is spanned by antisymmetrized products of the single-site, high-spin states. In the computations we have used the particle−hole relationship.[29] The ferrous and ferric sites contain four holes and five holes, respectively (Figure 1), such that each ferric site contains an itinerant hole in its non-indexed orbital. We thus consider a $d^5-d^5-d^4-d^4$ hole configuration. Since we are dealing with a four-spin problem, considerable freedom exists in the choice of the spin-coupling scheme used in the definition of the basis states. We adopt the following basis for the numerical analyses.

$$|((S_i,S_j)S_{ij},(S_k^0,S_l^0)S_{kl}^0)S_{\text{cube}}\rangle \qquad (1)$$

where $\{i, j, k, l\} = \{A, B, C, D\}$, $\{A, C, B, D\}$, $\{A, D, C, B\}$, $\{B, C, A, D\}$, $\{B, D, A, C\}$, and $\{C, D, A, B\}$. The notation $(S_A,S_B)S_{AB}$ stands for standard spin vector coupling of the spins S_A and S_B into resultant spin S_{AB}. The basis functions are characterized by the positions of the ferric sites containing the itinerant holes, the total cubane spin S_{cube}, which can range from 0 to 9, and the values of the intermediate spins $S_{ij}{}^0$ and S_{kl}, which are constrained by the common triangular inequalities.

Effective Hamiltonian. Electronic structure calculations of paramagnetic transition-ion clusters starting from the basic electrostatic two-particle interactions face considerable problems of both methodological and computational nature. On the other hand, phenomenological approaches are quite feasible and

(25) Cline, J. F.; Janick, P. A.; Siegel, L. M.; Hoffman, B. M. *Biochemistry* **1985**, *24*, 7942−7947.
(26) (a) Bertini, I.; Briganti, F.; Luchinat, C.; Scozzafava, A. *Inorg. Chem.* **1990**, *29*, 1874−1880. (b) Banci, L.; Bertini, I.; Luchinat, C. *Structure and Bonding*; Springer: Berlin, Heidelberg, 1990; Vol. 72, pp 113−136.
(27) Cai, L.; Holm, R. H. *J. Am. Chem. Soc.* **1994**, *116*, 7177−7188.
(28) Piepho, S. B.; Krausz, E. R.; Schatz, P. N. *J. Am. Chem. Soc.* **1978**, *100*, 2996−3005.
(29) Griffith, J. S. *The Theory of Transition Metal Ions*; Cambridge University Press: Cambridge, England, 1961.

provide, moreover, a clearer insight into the basic mechanisms underlying the essential features of these systems.

In the present work, the fundamental interactions are described by an effective Hamiltonian, $H_{eff} = H_t + H_{HDVV} + H_{vib} + H_{el}$, that incudes terms for hole transfer, HDVV exchange, vibronic interaction, and elastic energy of nuclear vibrations, respectively.

H_t is a one-particle operator that transfers itinerant holes between the localized orbital states at the metal sites of the cluster, thereby multiplying the resulting states by transfer parameters. By its action, the transfer operator may couple parallel the core spins of polynuclear clusters containing a single itinerant electron, a phenomenon which is usually referred to as double exchange.[2] The transfer operator considered here acts only on the holes in orbitals a, b, c, and d and can be written as[30]

$$H_t = \beta_0 P_0 \sum_{i<j} t_{ij} P_0 \tag{2}$$

where P_0 is the projector on the spin space of Hund's rule obeying states. The action of the pair transfer operators, t_{ij}, on two-hole states, $|kl\rangle$, obeying the Pauli principle $|lk\rangle = -|kl\rangle$, is defined by

$$t_{ij}|kl\rangle = \delta_{ik}|jl\rangle + \delta_{il}|kj\rangle + \delta_{jk}|il\rangle + \delta_{jl}|kj\rangle \qquad (i,j,k,l = a,b,c,d) \tag{3}$$

The matrix elements of the transfer operator between states including core spins can be evaluated by straightforward generalization of the technique given in ref 1b. When we consider a system of perfect T_d symmetry, the transfer interactions in the equivalent orbital pairs, (a,b), (a,c), ..., (c,d), are described by a single transfer parameter, β_0. The sign of the hole-transfer parameter, β_0, is opposite to that of the corresponding electron-transfer parameter.[29]

The HDVV operator, in T_d symmetry, describing the intercenter exchange interactions can be written as

$$H_{HDVV} = \sum_{\substack{i,j=1 \\ i<j}}^{4} \{J_{22}\vec{S}_i\cdot\vec{S}_j(1-n_i)(1-n_j) + J_{23}\vec{S}_i\cdot\vec{S}_j[n_i(1-n_j) + (n_i-1)n_j] + J_{33}\vec{S}_i\cdot\vec{S}_j n_i n_j\} \tag{4}$$

The HDVV Hamiltonian given in eq 4 accounts for the different values of the exchange-coupling constants in ferrous−ferrous (J_{22}), ferrous−ferric (J_{23}), and ferric−ferric (J_{33}) pathways. The occupation number n_i (i = A, B, C, D) keeps track of the centers containing the itinerant hole, i.e., $n_i = 1$ if the hole is on site i (ferric) and zero otherwise (ferrous). The HDVV operator is diagonal in the representation defined by eq 1, with the diagonal elements given by

$$E_{HDVV} = E_0 + \frac{(J_{33}-J_{23})}{2}S_{ij}(S_{ij}+1) + \frac{(J_{22}-J_{23})}{2}S^0_{kl}(S^0_{kl}+1) + \frac{J_{23}}{2}S_{cube}(S_{cube}+1) \tag{5}$$

Here E_0 is a spin-independent constant and i, j are labeling the ferric sites and k, l the ferrous sites in the basis state considered. E_0 is taken as zero in all calculations.

In homovalent binuclear compounds with paramagnetic sites, d^n-d^n, second-order electron-transfer interactions with $d^{n-1}-d^{n+1}$ configurations give rise to antiferromagnetic exchange couplings, $J_{AF} \sim \beta^2/U$, where β stands for an intermetal transfer parameter and U for the excitation energy.[31] If the transfer parameters involve ligand pathways, which is usually the case, the resulting spin coupling is referred to as superexchange. The β parameters depend considerably on structure. This dependence is believed to cause the strong magneto−structural correlations of the exchange interactions that are observed in a number of structurally related polynuclear complexes.[32] Similarly, it is to be expected that the parameter, β_0, for itinerant-electron transfer also depends significantly on structure. In our treatment of the [Fe$_4$S$_4$]$^{2+}$ cluster, we make the simplifying assumption that the transfer parameter is a function of one single structure parameter, r_{ij}, for each pair of sites (i,j): $\beta_{ij} = \beta_{ij}(r_{ij})$. In the initial T_d symmetric structure, $r_{ij} = r_{ij}^0$ for all pairs (i,j) for which $\beta_{ij}(r_{ij}^0) = \beta_0$. First-order expansion of β_{ij} around r_{ij}^0 yields

$$\beta_{ij} = \beta_0 + \Lambda\Delta r_{ij} \qquad (i,j = a,b,c,d) \tag{6}$$

With inclusion of pair-dependent β values, the transfer operator can be written as $H'_t = H_t + H_{vib}$, where H_t is defined by eq 2 and H_{vib} is given by

$$H_{vib} = P_0 \sum_{\substack{i,j=1 \\ i<j}}^{4} \Lambda\Delta r_{ij} t_{ij} P_0 \tag{7}$$

Since the operator in eq 7 gives rise to distortion-dependent interactions between the electronic states obtained in T_d symmetry, it is termed the vibronic coupling operator; Λ is the vibronic coupling constant. Multicenter vibrations of this type have been considered as a possible rationale for the interpretation of intervalence bandshapes in binuclear compounds.[33] The distortions Δr_{ij} are accompanied by deformation energies that are described by

$$H_{el} = \frac{1}{2}\kappa \sum_{\substack{i,j=1 \\ i<j}}^{4} \Delta r_{ij}^2 \tag{8}$$

where κ is a force constant. For convenience, we pass to coordinates (Q_i) adapted to T_d symmetry, eq 9. The symmetrized coordinates transform as a_1 (Q_a), e (Q_θ, Q_ϵ), and t_2 (Q_x, Q_y, Q_z) in T_d. The distortions Q_a represent a uniform change of the r_{ij} values. The e and t_2 distortions are illustrated in Figure 2, where, as an example, r_{ij} stands for an iron−iron distance.

$$\begin{pmatrix} Q_a \\ Q_\theta \\ Q_\epsilon \\ Q_x \\ Q_y \\ Q_z \end{pmatrix} = \begin{vmatrix} \frac{1}{\sqrt{6}} & \frac{1}{\sqrt{6}} & \frac{1}{\sqrt{6}} & \frac{1}{\sqrt{6}} & \frac{1}{\sqrt{6}} & \frac{1}{\sqrt{6}} \\ \frac{1}{\sqrt{3}} & -\frac{1}{2\sqrt{3}} & -\frac{1}{2\sqrt{3}} & -\frac{1}{2\sqrt{3}} & -\frac{1}{2\sqrt{3}} & \frac{1}{\sqrt{3}} \\ 0 & \frac{1}{2} & -\frac{1}{2} & -\frac{1}{2} & \frac{1}{2} & 0 \\ \frac{1}{\sqrt{2}} & 0 & 0 & 0 & 0 & -\frac{1}{\sqrt{2}} \\ 0 & \frac{1}{\sqrt{2}} & 0 & 0 & -\frac{1}{\sqrt{2}} & 0 \\ 0 & 0 & \frac{1}{\sqrt{2}} & -\frac{1}{\sqrt{2}} & 0 & 0 \end{vmatrix} \begin{pmatrix} \Delta r_{AB} \\ \Delta r_{AC} \\ \Delta r_{AD} \\ \Delta r_{BC} \\ \Delta r_{BD} \\ \Delta r_{CD} \end{pmatrix} \tag{9}$$

(30) Blondin, G.; Girerd, J.-J. *Chem. Rev.* **1990**, *90*, 1359−1376.

(31) Anderson, P. W. In *Magnetism*; Rado, G. T., Suhl, H., Eds.; Academic Press: New York, 1963; Vol. 1, Chapter 2, pp 25−83.

(32) *Magneto-Structural Correlations In Exchange-Coupled Systems*; Willett, R. D., Gatteschi, D., Kahn, O., Eds.; Reidel: Dordrecht, 1985.

(33) Piepho, S. B. *J. Am. Chem. Soc.* **1990**, *112*, 4197−4206.

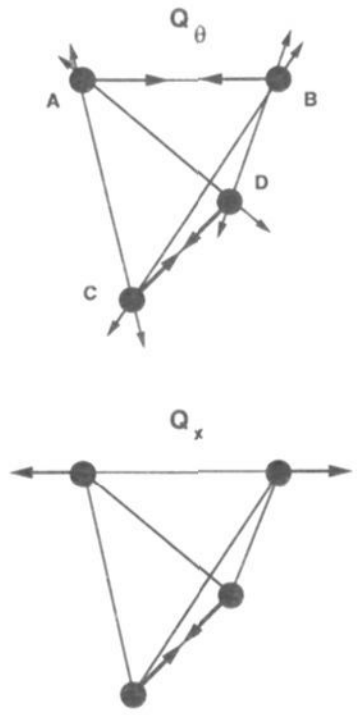

Figure 2. Symmetrized vibrations Q_θ (e symmetry) and Q_x (t_2 symmetry). Arrows indicate simultaneous displacements of the iron centers. Structure parameters, r_{ij}, are here interpreted as $Fe_i - Fe_j$ distances; alternative interpretations are possible (see text).

Table 1. Energy Eigenvalues of the Transfer Operator in the System $d^5-d^5-d^4-d^4$ in T_d Symmetry

S_{cube}	energy/β_0 (multiplicity)				dimension
0	−2 (6)	0 (19)		12/5 (5)	30
1	−2 (15)	−1/5 (32)	2/5 (19)	12/5 (12)	78
2	−2 (21)	−2/5 (39)	3/5 (32)	12/5 (16)	108
3	−2 (24)	−3/5 (40)	4/5 (39)	12/5 (17)	120
4	−2 (24)	−4/5 (35)	1 (40)	12/5 (15)	114
5	−2 (21)	−1 (24)	6/5 (35)	12/5 (10)	90
6	−2 (15)	−6/5 (15)	7/5 (24)	12/5 (6)	60
7	−2 (10)	−7/5 (8)	8/5 (15)	12/5 (3)	36
8	−2 (6)	−8/5 (3)	9/5 (8)	12/5 (1)	18
9	−2 (3)			2 (3)	6

The Q-dependence of the electronic energies can be explored by performing numerical diagonalizations of the matrices of H_{eff} at the points of a grid in the Q-space. The energy minimum of the lowest adiabatic potential well, obtained for a given value of S_{cube}, defines in semiclassical approximation the stable nuclear configuration and the spin structure for this spin value. The minima were ascertained by a numerical simplex method for all possible values of S_{cube}. The results will be analyzed in the next section.

Results for $[Fe_4S_4]^{2+}$

Eigenvalues of H_t. The energy eigenvalues of the transfer operator in the system $d^5-d^5-d^4-d^4$ are given in Table 1. The ground manifold is highly degenerate. For $\beta_0 > 0$, it has energy $-2\beta_0$ and includes spin states ranging from $S_{cube} = 0$ to 9, while S_{cube} ranges from 0 to 8 for $\beta_0 < 0$. Furthermore, the ground states of given spin S_{cube} have degeneracies ranging from 1 to 24, providing the prerequisite for Jahn−Teller distortion.[34] The degeneracies are partially removed by introducing HDVV exchange with different values for the coupling constants J_{22}, J_{23}, and J_{33}. For $\beta_0 > 0$, the 6-fold degeneracy of the ground state with $S_{cube} = 0$ is split into $2A_i + 2E$ (T_d), while for $\beta_0 < 0$, the $S_{cube} = 0$ ground manifold is split into $A_i + 2E$.

Broken-Symmetry States for $\beta_0 > 0$. For $\beta_0 > 0$, the analysis of the adiabatic potential surface for the ground state

(34) (a) Bersuker, I. B. *The Jahn−Teller Effect and Vibronic Interactions in Modern Chemistry*; Plenum: New York, 1984. (b) Bersuker, I. B.; Borshch, S. A. In *Advances in Chemical Physics*; Prigogine, I., Rice, S. A., Eds.; John Wiley: New York, 1992; Vol. 81, pp 703−782.

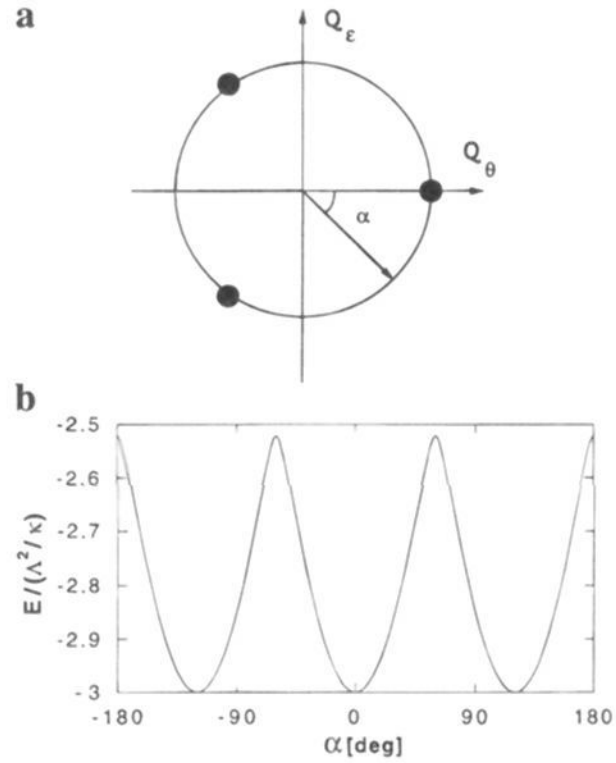

Figure 3. (a) Plane in vibrational space defined by $((3/2)^{1/2}\ \Lambda/\kappa, Q_\theta, Q_\epsilon, 0, 0, 0)$. The circle indicated is centered at $Q_\theta = Q_\epsilon = 0$ and has radius $R = (4/3)^{1/2}\ \Lambda/\kappa$. The positions of adiabatic potential-well minima calculated for $\beta_0 > 0$ are indicated by dots. The positions are independent of S_{cube}. The angle α parametrizes the circumference of circle. (b) Section of the adiabatic potential surface calculated in $S_{cube} = 0$ state using $\beta_0 = \Lambda^2/\kappa > 0$ and $J_{22} = J_{23} = J_{33} = 0$ along the circle defined in (a).

with $S_{cube} = 0$ yields the following results. The distortions of t_2 symmetry are Jahn−Teller inactive, i.e., $Q_x = Q_y = Q_z = 0$ at the minima of the adiabatic potential well. This property is imposed by symmetry: thus, $\langle X|t_2|Y\rangle = 0$ for X, Y = A_i or E according to the reduction table for products of irreducible representations of the T_d group.[35] Figure 3b presents a section of the adiabatic potential surface for $S_{cube} = 0$ and $\beta_0 = \Lambda^2/\kappa$ along a circle in the e-space centered at $Q_a = (2/3)^{1/2}\ \Lambda/\kappa$ ($Q_\epsilon = Q_\theta = Q_x = Q_y = Q_z = 0$) and radius $R = (4/3)^{1/2}\ \Lambda/\kappa$, shown in Figure 3a. The potential well has three equivalent minima with energy $-3\Lambda^2/\kappa$ which are separated by three thresholds of height ca. $0.5\Lambda^2/\kappa$. A similar type of potential surface was found for the $d^5-d^5-d^6$ system.[1a,c] The vectors (r_{AB}, r_{AC}, r_{AD}, r_{BC}, r_{BD}, r_{CD}) defining the minima are given by (Λ/κ, 0, 0, 0, 0, Λ/κ), (0, Λ/κ, 0, 0, Λ/κ, 0), and (0, 0, Λ/κ, Λ/κ, 0, 0), indicating that the distortions occur in separate pairs, (A,B) and (C,D), ..., whereas the interlayer distortions are zero. Hence, the T_d symmetry is lowered to D_{2d} symmetry by Jahn−Teller distortion. The same symmetry breaking is obtained for the ground states with $S_{cube} > 0$.[36] Thus, this type of symmetry breaking can already be found in the simplest cubane containing two itinerant particles.[37] Analysis of the electronic ground states in the distorted structures reveals that each of the itinerant holes is delocalized over one of the pairs. At each minimum, the system can be considered as consisting of two mixed-valence dimers, each with maximum dimer spin due to double exchange. The

(35) Wilson, E. B.; Decius, J. C.; Cross, P. C. *Molecular Vibrations*; Dover: New York, 1980.

(36) Ground states of H_t for $S_{cube} > 0$ contain T_i states that are coupled by distortions of t_2 symmetry. For instance, the electronic space for $S_{cube} = 9$ can be decomposed as $T_1 + T_2$. These triplets are split in energy (ΔE) into a singlet (ground) and a doublet at the D_{2d} minima indicated in Figure 3a. Treating the pseudo-Jahn−Teller t_2 couplings between the split T_i states in second-order perturbation theory leads to energy corrections of the form $-c_iQ_i^2$ ($c_i > 0$, $i = x, y, z$), with $c_i \sim 1/\Delta E$. The splittings of the T_i levels are sufficiently large in order to secure that the c_i values are smaller than $\kappa/2$, such that the "effective" force constants $K_i = \kappa/2 - c_i$ (in $K_iQ_i^2$) are positive, thus preventing the system from distorting along the Q_i coordinates of t_2 symmetry.

(37) The vibronic problem for $S_{cube} = 9$ is identical to that of the $S_{cube} = 1$ state of the system $d^1-d^1-d^0-d^0$.

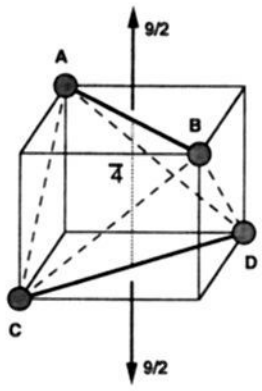

Figure 4. Schematic representation of the Jahn−Teller distorted D_{2d} structure and of the diamagnetic ground state at a minimum of adiabatic potential well for $\beta_0 > 0$. Strengths of resonance interactions are indicated by boldface lines for the strong interaction (β_{intra}) and broken lines for the weaker interaction (β_{inter}). Delocalized-pair spins are given by arrows.

pair spins in the broken-symmetry state with $S_{cube} = 0$ are antiparallel as shown in Figure 4. The ground state energies are independent of S_{cube} for positive β_0 and are the sum of two identical contributions, one from each pair. The pair energies can be decomposed into three contributions,

$$E_{pair} = -\beta_0 - \frac{\Lambda^2}{\kappa} + \frac{\Lambda^2}{2\kappa} \qquad (10)$$

for hole transfer (H_t), for vibronic coupling, representing the enhancement of the delocalization energy in the pairs due to the Jahn−Teller distortion (H_{vib}), and for elastic deformation (H_{el}), respectively.

The electron delocalization problem of a particle in a high-spin (spin 9/2), mixed-valence Fe dimer is equivalent to the problem of a dimer containing a single itinerant particle. Therefore, the itinerant holes in the broken-symmetry ground states are moving, for $\beta_0 > 0$, in orbitals of the type $\phi_{ab}^- = (|a\rangle - |b\rangle)/\sqrt{2}$, $\phi_{cd}^- = (|c\rangle - |d\rangle)/\sqrt{2}$ which are eigenfunctions of *intra*-pair transfer operators t_{ab} and t_{cd} with energies $-\beta_0$. On the other hand, the action of the *inter*-pair transfer operator yields zero, e.g.,[1c,d]

$$[t_{ac} + t_{ad} + t_{bc} + t_{bd}]\phi_{ab}^- = 0 \qquad (11)$$

In other words, interlayer resonance does not contribute to the energy. Hence, the "layered" states are eigenstates of the transfer operator H_t with total resonance energy $-2\beta_0$. The 6-fold degenerate ground state of the transfer operator contains three layered states which can be locked-in by vibronic coupling, i.e. the latter states are lowered in energy relative to the other three states which have a more complex composition. By combining H_t and H_{vib}, one distinguishes, due to the D_{2d} symmetry, effective parameters for intra- and interpair transfer, which, at the minima, can be written as

$$\beta_{intra} = \beta_0 + \frac{\Lambda^2}{\kappa} \quad \text{and} \quad \beta_{inter} = \beta_0 \qquad (12a)$$

Calculations performed for different values of β_0 reveal that the condition for the symmetry breaking from T_d to D_{2d} is $\Lambda^2/\kappa \neq 0$. Hence, delocalized-pair formation does not require that β_{inter} is small compared to β_{intra}.

The stability of the broken-symmetry states against t_2 distortions can now be understood in more physical terms. Let us consider t_2 distortions away from one of the minima: $((2/3)^{1/2}\,\Lambda/\kappa, -(4/3)^{1/2}\,\Lambda/\kappa, 0, Q_x, Q_y, Q_z)$. As Q_a, Q_θ, and Q_ϵ are kept constant under distortion, $r_{AB} + r_{CD}$ remains constant as well. Then, changes along $Q_x = (r_{AB} - r_{CD})/\sqrt{2}$ only allow

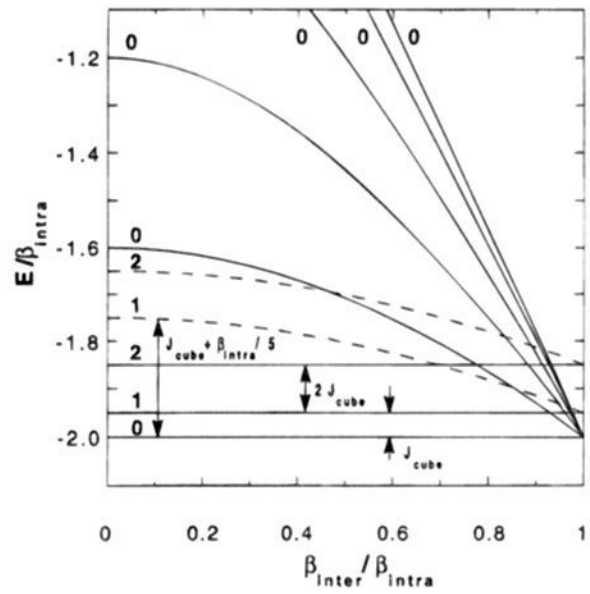

Figure 5. Energy level diagram of the Hamiltonian $H'_t + H_{HDVV}$ displaying the lowest eigenstates with spin $S_{cube} = 0$, 1, and 2 as a function of $\beta_{inter}/\beta_{intra}$. Also given are the energies of the next five $S_{cube} = 0$ states. The broken curves show the energies of the lowest excited $S_{cube} = 1$ and 2 states. The latter states are doubly degenerate and are of the form $|(9/2,7/2)S_{cube})\rangle$ for $\beta_{inter}/\beta_{intra} \approx 0$. Parameters used: $\beta_{intra} = 4000$ cm^{-1}, $J_{22} = J_{23} = J_{33} = 200$ cm^{-1}.

the values $r_{AB} + \Delta r$ and $r_{CD} - \Delta r$. The corresponding changes in β_{intra}, $+\Lambda\Delta r$ for (A,B) and $-\Lambda\Delta r$ for (C,D), cancel in the calculation of the net delocalization energy. Changes in Q_y and Q_z affect only β_{inter} and do not alter the energy of the pair-delocalized state either. Hence, t_2 distortions from D_{2d} symmetry cost only elastic deformation energy without getting any delocalization energy in return and are therefore disfavored.

The results of the minimizations are only insignificantly affected by HDVV exchange. However, its effect on the relative spin multiplet energies is significant.

Excited State Energies for $\beta_0 > 0$. As mentioned above, the ground state energy pertaining to $H_t + H_{vib} + H_{el}$ is independent of the total spin, S_{cube}. We now consider the relative state energies in the presence of HDVV exchange as obtained at the minima of the adiabatic potential for $S_{cube} = 0$. If ground- and excited-state energies are evaluated at an arbitrary, fixed point in Q-space, the elastic energy term will be a constant common to all states and can thus be ignored in considering relative energies. As shown above, the minima of the adiabatic potential occur at three equivalent points in Q-space. The coordinates of these points, $Q_i/(\Lambda/\kappa)$, are independent of β_0. The value of β_0 in units Λ^2/κ corresponds to a unique value for the ratio $\beta_{inter}/\beta_{intra}$ which follows from eq 12a

$$\frac{\beta_{inter}}{\beta_{intra}} = \frac{\dfrac{\beta_0}{\Lambda^2/\kappa}}{\dfrac{\beta_0}{\Lambda^2/\kappa} + 1} \qquad (12b)$$

The β-ratio is 0 for $\beta_0 = 0$ and approaches 1 in the limit where the vibronic stabilization energy, Λ^2/κ, becomes a vanishing correction to the delocalization energy, $-2\beta_0$. Since accurate experimental data for β_0 and Λ^2/κ are lacking (see below), it is worthwile to extend our theoretical considerations to the full range $0 < \beta_0/(\Lambda^2/\kappa) < \infty$, for which $0 < \beta_{inter}/\beta_{intra} < 1$ according to eq 12b.

Figure 5 presents lowest energy eigenvalues of $H'_t + H_{HDVV}$ for $S_{cube} = 0$, 1, and 2 in D_{2d} symmetry as obtained in the presence of homogeneous HDVV exchange (i.e., $J_{22} = J_{23} = J_{33} \equiv J_{cube}$) of antiferromagnetic sign ($J > 0$) as a function of the ratio $\beta_{inter}/\beta_{intra}$.[38] The figure shows that antiferromagnetic exchange stabilizes a diamagnetic ground state ($S_{cube} = 0$). As

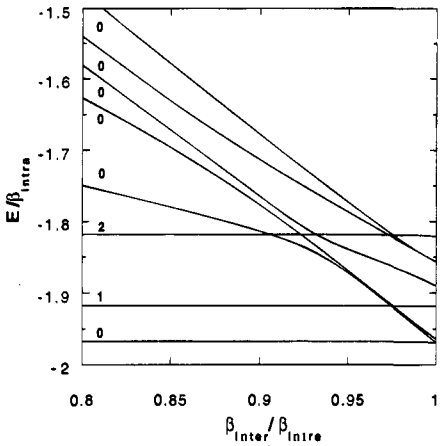

Figure 6. Energy level diagram of the Hamiltonian $H'_1 + H_{HDVV}$ displaying the lowest eigenstates with spin $S_{cube} = 0$, 1, and 2 as a function of $\beta_{inter}/\beta_{intra}$ obtained by using different values for the exchange-coupling constants between the ferrous−ferrous (J_{22}), ferrous−ferric (J_{23}), and ferric−ferric (J_{33}) sites. Also given are the energies of the next five $S_{cube} = 0$ states; higher-lying paramagnetic states are not shown. Parameters used: $\beta_{intra} = 4000$ cm^{-1}, $J_{22} = 80$ cm^{-1}, $J_{23} = 160$ cm^{-1}, and $J_{33} = 360$ cm^{-1}.

expected for homogeneous exchange, the excited states lie at $E = J_{cube}$ for $S_{cube} = 1$ and $E = 3J_{cube}$ for $S_{cube} = 2$ above the ground state throughout the β-ratio range. The two states result from spin coupling of the two delocalized spin 9/2 moieties: $|(9/2,9/2)\, S_{cube}\rangle$. Furthermore, the figure shows the energies of the five lowest excited states with $S_{cube} = 0$. These energies merge with the ground state into a 6-fold degenerate set at $\beta_{inter}/\beta_{intra} = 1$ (see also Table 1). Also shown are the next higher lying states of spin $S_{cube} = 1$ and 2. These states belong to degenerate manifolds of multiplicity 15 ($S_{cube} = 1$) and 21 ($S_{cube} = 2$) in the weak coupling limit. We note in passing that the minima in the adiabatic potential wells for excited states do not coincide, in general, with the locations of the minima in the well for the ground state.

Figure 6 presents the energies in the presence of inhomogeneous HDVV exchange ($J_{22} < J_{23} < J_{33}$). The energy gaps between the ground state and the excited states are approximately given by $\Delta E = J_{cube}$ for $S_{cube} = 1$ and $\Delta E = 3J_{cube}$ for $S_{cube} = 2$, where J_{cube} is an averaged coupling constant connecting the Fe sites in different pairs. Figure 6 shows that four of the diamagnetic states, including the ground state, merge into two distinct doublets (E) in the limit $\beta_{inter}/\beta_{intra} = 1$.[38]

Values of Model Parameters. Our theoretical model depends essentially on five parameters: the electron-transfer parameter, β_0, the vibronic energy, Λ^2/κ, and the exchange-coupling constants for ferrous−ferrous, ferrous−ferric, and ferric−ferric exchange (J_{22}, J_{23}, and J_{33}). Experimental data are available for the J-values of the $[Fe_2S_2]^{2+}$ cores found in proteins and synthetic analogs. Magnetic susceptibility studies suggest $J_{33} = 296$ cm^{-1} for $[Fe_2S_2(SR)_4]^{2-}$,[39a] $J_{33} = 316$ cm^{-1} for $[Fe_2S_2(Cl)_4]^{2-}$,[13a] and $J_{33} = 366$ cm^{-1} for the cluster in oxidized spinach ferredoxin.[40] Furthermore, room-temperature values for the magnetic moment have been reported to lie in the range $1.4\ \mu_B \le \mu_{eff}/Fe \le 1.9\ \mu_B$,[39b,c] corresponding to exchange-coupling constants 190 cm$^{-1} \le J_{33} \le 310$ cm^{-1} as defined by $H = J_{33}\vec{S}_1\cdot\vec{S}_2$. The magnetic moment, $\mu_{eff}/Fe \approx 1.4\ \mu_B$, of the site-differentiated cubane cluster $[Fe_4S_4L_2(RCN)_6]^{2+}$, containing two low-spin Fe^{2+} sites and two antiferromagnetically coupled high-spin Fe^{3+} sites, suggests the value $J_{33} \approx 310$ cm^{-1}.[41]

To date, no synthetic analogs containing $[Fe_2S_2]^{1+}$ cores have been magnetically characterized. However, J_{23} for spinach ferredoxin has been reported as $J_{23} \le 198$ cm^{-1},[40] while a lower bound, $J_{23} \ge 160$ cm^{-1}, is given in ref 42. In general, the constants for ferric−ferric coupling are found to be larger than those for the mixed-valent dimers. For the calculations with inhomogeneous exchange, we have adopted the values $J_{23} = 160$ cm^{-1} and $J_{33} = 360$ cm^{-1} as well as an extrapolated value of 80 cm^{-1} for J_{22}, while in calculations with homogeneous exchange we took the average $J_{cube} = 200$ cm^{-1}.

Theoretical studies report β-values ranging from 1000 to 6000 cm^{-1}.[43,1c] By adopting $\beta_{intra} = 4000$ cm^{-1}, one obtains the ratio $J_{cube}/\beta_{intra} = 0.05$ used in Figure 5 and the ratios $J_{22}/\beta_{intra} = 0.02$, $J_{23}/\beta_{intra} = 0.04$, and $J_{33}/\beta_{intra} = 0.09$ used in Figure 6. Neither experimental nor theoretical data are available for the quantity Λ^2/κ of the $[Fe_4S_4]^{2+}$ cluster. The lack of these data for β_0 and Λ^2/κ is, however, of little consequence for our considerations, since the principal conclusions do not depend sensitively on their values.

Broken-Symmetry States for $\beta_0 < 0$. The energies listed in Table 1 show that the ground state space of the transfer operator for $\beta_0 < 0$ is highly degenerate, with energy $-12\beta_0/5$. This manifold includes states with $S_{cube} = 0 - 8$. The 5-dimensional ground state for $S_{cube} = 0$ can be decomposed as $A_i + 2E(T_d)$, such that the coordinates of t_2 symmetry are Jahn−Teller inactive as in the case of $\beta_0 > 0$. The analyses of the adiabatic potential wells for $S_{cube} = 0-8$ indicate that the minima are attained at three equivalent structures of D_{2d} symmetry. At the minima, we are again essentially dealing with two delocalization parameters, β_{inter} and β_{intra}. Although the symmetry of the distorted structures is independent of the sign of β_0, the positions in Q-space of the minima obtained for $\beta_0 < 0$ differ from those for $\beta_0 > 0$. This can be seen by comparing the plot of the relationship between $\beta_0 < 0$ and the value of the ratio $\beta_{inter}/\beta_{intra}$ calculated at the well minima with the plot of the relationship for $\beta_0 > 0$ given in eq 12b (Figure 7). The difference can be interpreted as follows.[1d] The itinerant hole particle in the high-spin ground state of an isolated dimer with the hole configuration d^4-d^5 is described by a symmetric orbital, say $(|a\rangle + |b\rangle)/\sqrt{2}$, for $\beta_0 < 0$. As a consequence, eq 11 has to be replaced by

$$[t_{ac} + t_{ad} + t_{bc} + t_{bd}]\phi^+_{ab} = 2\phi^+_{cd} \qquad (13)$$

in the analysis of the tetramer. Two non-interacting, high-spin dimers are not, as for $\beta_0 > 0$, an eigenstate of H_1: there is also "interlayer" resonance with configurations in which the two itinerant holes are stored in the same pair. As a consequence, the resonance energy in the ground state is by $|2\beta_0/5|$ larger than for $\beta_0 > 0$ (Table 1).[44] As the interlayer linkages furnish a part of the delocalization energy, the system can gain vibronic

(38) It should be noted that Figures 5 and 6 depict only a fraction of the states that are actually present in the energy ranges shown in these figures.

(39) (a) Gillum, W. O.; Frankel, R. B.; Foner, S.; Holm, R. H. *Inorg. Chem.* **1976**, *15*, 1095−1100. (b) Cleland, W. E.; Averill, B. A. *Inorg. Chem.* **1984**, *23*, 4192−4197. (c) Salifoglou, A.; Simopoulos, A.; Kostikas, A.; Dunham; R. W.; Kanatzidis, M. G.; Coucouvanis, D. *Inorg. Chem.* **1988**, *27*, 3394−3406.

(40) Palmer, G.; Dunham, W. R.; Fee, J. A.; Sands, R. H.; Iizuka, T.; Yonetani, T. *Biochim. Biophys. Acta* **1971**, *245*, 201−207.

(41) Goh, C.; Weigel, J. A.; Holm, R. H. *Inorg. Chem.* **1994**, *33*, 4861−4868.

(42) Bertrand, P.; Guigliarelli, B.; More, C. *New J. Chem.* **1991**, *15*, 445−454.

(43) Noodleman, L.; Case, D. A. In *Advances in Inorganic Chemistry*; Sykes, A. G., Ed.; Academic Press: New York, 1992; Vol. 38, pp 423−470.

(44) The result for the increment can be generalized to the system $\phi_L{}^{n+1} - \phi_L{}^{n+1} - \phi_L{}^n - \phi_L{}^n$, where the ϕ_L stand for P, D, F, ... shells (L = 1, 2, 3, ...) and $n = 2L$, by the expression $-2\beta_0/(n+1)$. Thus, in the limit, $n \to \infty$, the interlayer resonance vanishes.

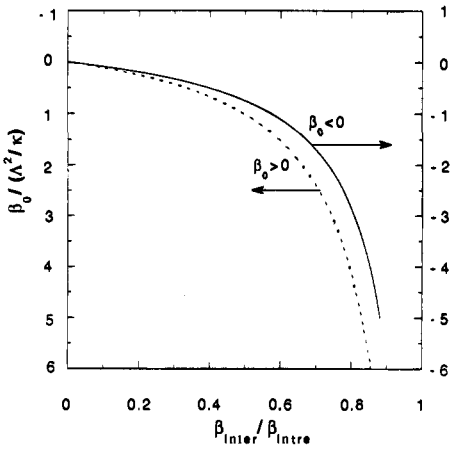

Figure 7. Relationships $\beta_0/(\Lambda^2/\kappa)$ versus $\beta_{inter}/\beta_{intra}$ as obtained at the minima of the adiabatic potential wells for the lowest $S_{cube} = 0$ state in the range of negative β_0 values (right-hand scale). The broken curve gives the relationship of β_0 versus $\beta_{inter}/\beta_{intra}$ given in eq 12b in the range of positive $\beta_0/(\Lambda^2/\kappa)$ values (left-hand scale). J_{22}, J_{23}, and J_{33} have been taken as zero.

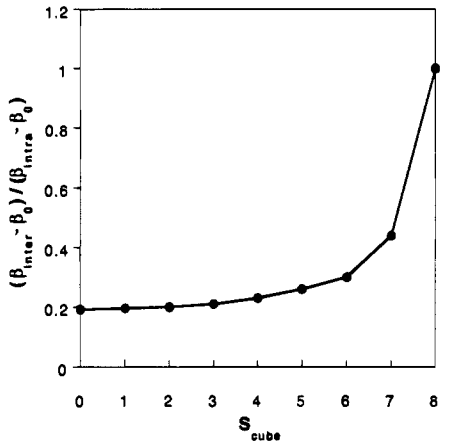

Figure 8. Ratio of the vibronic changes in the values of β_{inter} and β_{intra} as a function of S_{cube} calculated at the minima of lowest adiabatic potential wells for these spins. Parameters used: $\beta_0 = -5\Lambda^2/\kappa$ and $J_{22} = J_{23} = J_{33} = 0$.

energy by distorting the coordinates r_{AC}, r_{AD}, r_{BC}, and r_{CD} as well. Concomitantly, the distortions r_{AB} and r_{CD} are somewhat reduced, such that the ratio $\beta_{inter}/\beta_{intra}$ is enhanced relative to its value for $|\beta_0|$ (eq 12b), as can be observed in Figure 7. The contribution from interlayer resonance to the ground state energy increases monotoneously with increasing spin ($S_{cube} < 9$), because the relative orientation of the pair spins changes from antiparallel to parallel. In other words, the delocalization energy is more "localized" (on the two pairs) in states of lower spin. Consequently, the distortion-induced changes in β_{inter} (i.e., $\beta_{inter} - \beta_0$) increase relative to the distortion-induced changes in β_{intra} (i.e., $\beta_{intra} - \beta_0$) in the order of increasing spin (Figure 8). The optimal vibronic energy gain is attained in states where the resonance energy is "localized" in a small number of linkages. Therefore, the largest vibronic stabilization energy results for $S_{cube} = 0$, with excited states occurring in the order $S_{cube} = 1$, 2, ... (Figure 9). The combination of electron-transfer interaction and vibronic coupling thus leads to an effective exchange-coupling mechanism stabilizing a diamagnetic ground state for $\beta_0 < 0$. A similar effective spin-coupling mechanism has been reported in systems containing a single itinerant electron for β_0 values of opposite sign, $\beta_0 > 0$.[1c,d] The sign flip of β_0 needed to secure the "vibronic spin coupling" is due to the hole formalism adopted in the present work.

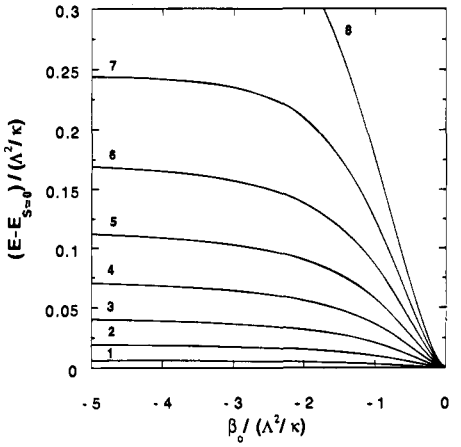

Figure 9. Energies of broken-symmetry states calculated at the minima of the adiabatic potential wells obtained with the values for β_0 and S_{cube} indicated in the figure. The energy for $S_{cube} = 0$, $E_{S=0}$, has been taken as the zero point of the energy scale for every value of β_0 considered. J_{22}, J_{23}, and J_{33} have been taken as zero.

Excited States for $\beta_0 < 0$. For $\beta_0 < 0$, the lowest-lying energy levels (not shown) for $S_{cube} = 1$ and 2, over a wide range of $\beta_{inter}/\beta_{intra}$, are at energies of approximately J_{cube} and $2.5J_{cube} - 3J_{cube}$ above the diamagnetic ground state energy (J_{cube} is defined as the average of J_{22}, J_{23}, and J_{33} for which the same values were taken as in Figure 6; $\beta_{intra} = -4000$ cm^{-1}). As discussed above, the lowest levels with $S_{cube} = 0$, 1, ... are already nondegenerate in the absence of HDVV exchange for $-1 < \beta_{inter}/|\beta_{intra}| < 0$. However, the energy gaps caused by the vibronic interactions amount to only $\leq 4\%$ (between $S_{cube} = 0$ and 1) and $\leq 11\%$ (between 0 and 2) of the exchange splittings provided by the J terms (using the J values of Figure 6). The 5-fold degenerate ground state of the transfer operator in T_d symmetry ($\beta_{inter}/\beta_{intra} = 1$, see Table 1) is split in a singlet ground state and two $E(T_d)$ levels by the inhomogeneous HDVV interaction.

Discussion of Results for $[Fe_4S_4]^{2+}$

Comparison with Previous Work. In the preceding section, we have discussed a vibronic-coupling mechanism by which T_d-symmetric $[Fe_4S_4]^{2+}$ cores may undergo Jahn−Teller distortion to structures of D_{2d} symmetry. The Jahn−Teller effect as a possible rationale for symmetry lowering in $[Fe_4S_4]^{3+,2+}$ clusters has been discussed by Dahl et al.[45] and Carter et al.[46] The early treatments rest on closed-shell, molecular-orbital (MO) descriptions of the diamagnetic ground state of the $[Fe_4S_4]^{2+}$ cluster. Depending on the energy order of the MO's, the electron-filling scheme may possess a partially occupied t_2 orbital triplet at the top, leading to Jahn−Teller distortion. Partially filled top orbitals were found both in a qualitative fashion[45] and in closed-shell X_α calculations by Yang et al.[47] The structure adopted in the X_α calculations (Fe and S at the vertices of a cube) was criticized by Aizman and Case.[48] Using a more realistic structure, wherein the Fe and S sites are placed at the vertices of two concentric tetrahedra of different size, the latter authors obtained an MO scheme in which the top manifold is completely filled, and thus Jahn−Teller distortions

(45) (a) Trinh-Toan, Fehlhammer, W. P.; Dahl, L. F. *J. Am. Chem. Soc.* **1972**, *94*, 3389−3397. (b) Gall, R. S.; Chu, C. T. W.; Dahl, L. F. *J. Am. Chem. Soc.* **1974**, *96*, 4019−4023. (c) Simon, G. L.; Dahl, L. F. *J. Am. Chem. Soc.* **1973**, *95*, 2175−2183. (d) Simon, G. L.; Dahl, L. F. *J. Am. Chem. Soc.* **1973**, *95*, 2164−2174.

(46) Carter, C. W.; Kraut, J.; Freer, S. T.; Alden, R. A. *J. Biol. Chem.* **1974**, *249*, 6339−6346.

(47) Yang, C. Y.; Johnson, K. H.; Holm, R. H.; Norman, J. G. *J. Am. Chem. Soc.* **1975**, *97*, 6596−6598.

(48) Aizman, A.; Case, D. A. *J. Am. Chem. Soc.* **1982**, *104*, 3269−3279.

would not appear to be responsible for the descent from T_d symmetry. However, it is important to recognize that closed-shell MO theory is deficient in describing the strong *interionic* correlation of the 3d electrons at the paramagnetic sites of antiferromagnetically coupled clusters. Thus, conclusions concerning the Jahn−Teller effect in $[Fe_4S_4]^{n+}$ clusters drawn from application of closed-shell MO theory are likely to be of marginal importance. In our approach, the correlation of the 3d core electrons is accounted for by adopting valence-bond configurations based on Wannier-type orbitals as the starting point of the calculations. The effect of incipient intermetal delocalization of the paramagnetic core electrons on spin state energies is incorporated in our model by introducing antiferromagnetic exchange-coupling terms as described by P. W. Anderson.[31] In contrast to the closed-shell MO prediction that the Jahn−Teller effect should be absent, our results indicate that important structural distortions may arise in the framework of a correlated-electron theory.

Magnetic susceptibility data of $[Fe_4S_4]^{2+}$ clusters indicate the presence of one or more excited paramagnetic states at only a few hundred wavenumbers above the diamagnetic ground state.[8,13,15] Yang et al. proposed that an excited state, assumed to be a spin triplet, derives from excitation of an electron within the Jahn−Teller split t_2 top orbitals.[47] Having excluded such a possibility, Aizman and Case[48] considered an alternative interpretation of the excited state, which was prompted by a Mössbauer study of the $[Fe_4S_4]^{3+}$ cluster in HiPIP reported by Middleton et al.[7b] The latter study has suggested that the ^{57}Fe sites occur as two inequivalent pairs that can be approximately characterized as a delocalized $Fe^{2.5+}Fe^{2.5+}$ pair with spin 9/2 and an $Fe^{3+}Fe^{3+}$ pair with spin 4, the two dimer spins being coupled to a resultant spin $S_{cube} = 1/2$. Aizman and Case made the plausible assumption that an electron added upon reduction of the $[Fe_4S_4]^{3+}$ core will be accommodated in a second delocalized pair, the pair spins now being coupled by antiferromagnetic exchange to form a diamagnetic ground state. An HDVV exchange-coupling constant, $J_{cube} = 380\ cm^{-1}$, between the two Fe_2S_2 pairs was estimated by using broken spin-symmetry, unrestricted Hartree−Fock X_α calculations, leading to an excited $S_{cube} = 1$ state at energy $2J_{cube} = 760\ cm^{-1}$ above the ground state. The calculations presented here show that both the D_{2d} symmetry and the spin-state structure of the $[Fe_4S_4]^{2+}$ cluster postulated by Aizman and Case can be interpreted as the consequence of an interplay between double exchange and vibronic coupling.

Magnetic susceptibility studies on a number of $[Fe_4S_4]^{2+}$-containing models and proteins have been reported: $[Fe_4S_4(SCH_2Ph)_4]^{2-}$ and $[Fe_4S_4(SPh)_4]^{2-}$ ($J \approx 464\ cm^{-1}$),[8] $[Fe_4S_4Cl_4]^{2-}$ ($J = 440\ cm^{-1}$),[13a] $[Fe_4S_4(OPh)_4]^{2-}$ ($320\ cm^{-1} \leq J \leq 380\ cm^{-1}$),[13b] and $HiPIP_{red}$ ($J \geq 400\ cm^{-1}$).[15b] The coupling constants given in parentheses were obtained from fits of the data with a pure HDVV model using a single exchange-coupling constant for which the energies are $E(S_{cube}) = (J/2)S_{cube}(S_{cube} + 1)$. The spin levels of this model are, of course, highly degenerate. The application of the pure HDVV model encounters two problems. Thus, in no case were the fits found to be satisfactory over the entire temperature range, and moreover, the values obtained for J were at least twice as large as the valence-state-averaged coupling constant deduced from the magnetic data of dimeric clusters ($J_{cube} \approx 200\ cm^{-1}$). The two problems can be attributed to the high degeneracies of the first and higher excited $S_{cube} = 1, 2, \ldots$ states, which lead to sigmoidal shaped χT vs T plots that do not fit the almost linear behavior observed above 100 K and which, moreover, necessitate the use of large J values. Although the quality of the fits is improved by using an HDVV model with two exchange parameters, such a procedure yields even larger exchange-coupling constants ($J_{22} = 450\ cm^{-1}$ and $J_{33} = 550\ cm^{-1}$).[49] It should be pointed out that the susceptibilty data were analyzed prior to the recognition that double-exchange effects are important in these systems. In the light of the present and recent work, it seems more appropriate to describe the magnetic susceptibility data by a model that includes both resonance and vibronic interaction.

It may be useful to mention a few points regarding the analysis and interpretation of the magnetic data of $[Fe_4S_4]^{2+}$ clusters. (a) Double exchange reduces the degeneracies of the energy levels obtained with a pure HDVV model (see above). Magnetic data analyses that are based on effective Hamiltonian descriptions including double exchange allow for better fits and lower values of the coupling constants, J_{ij}. (b) As has been suggested by Jordanov *et al.*,[50] tetramers may have larger values for J_{22}, J_{23}, and J_{33} than the dimeric species. (c) The values for J_{23} derived from studies of dimeric species may contain ferromagnetic contributions due to incipient intermetal delocalization of the itinerant electron. In second-order perturbation theory, the delocalization effect on spin state energy is also described by the common HDVV Hamiltonian with an exchange-coupling constant, J_F, of ferromagnetic sign and therefore cannot be separated out from a compounded J_{23} value.[51] However, since in our treatment of the tetramer the itinerant electron delocalization is explicitly accounted for by the operator H_t, the empirical data for antiferromagnetic exchange-coupling constants in localized mixed-valence dimers must be corrected for the contribution J_F. The value for J_{23} to be used in our analysis may thus exceed the value of $160\ cm^{-1}$ by an unknown amount, which may have the effect of enhancing J_{cube} to values larger than $200\ cm^{-1}$. (d) In the case of weak vibronic coupling, the intrusion of $S_{cube} = 0$ states in the interval between the $S_{cube} = 1$ triplet and the ground state (see Figures 5 and 6) may require a reduction of J_{cube} in order to compensate for the Boltzmann occupation of the intruding diamagnetic states. Next to the paramagnetic states of the form $|(9/2,9/2)S_{cube}\rangle$ ($S_{cube} > 0$) an additional number of states (see Figure 5) may need to be considered in the analyses of NMR and magnetic data depending on the value for $\beta_{inter}/\beta_{intra}$.

In a recent series of papers on systems containing a single itinerant electron, the interplay of double exchange and vibronic coupling was proposed as a possible mechanism for the pair trapping of the itinerant electron.[1] The vibronic coupling mechanism studied in the previous work differs from the mechanism introduced here in that the former considers the coupling between symmetric local vibrations and inhomogeneous electronic charge distributions (the PKS mechanism).[28] Figure 10 (top) shows that the PKS distortions in the environments of a delocalized pair differ from those of an empty pair. The transfer of the itinerant electron to the empty pair at a fixed geometry (Figure 10, top right) yields a state of higher energy, which prevents a coherent superposition of the two states (i.e., the electron is trapped in the pair with the relaxed environments). However, as can be seen from Figure 10 (bottom), the three delocalization modes of a 2-electron system discussed above have equal distortion energies according to the PKS mechanism, since each Fe site contains formally half of an itinerant-electron charge. The inability of the PKS mechanism to break the T_d symmetry of the $[Fe_4S_4]^{2+}$ cluster follows also from the

(49) Papaefthymiou, G. C.; Laskowski, E. J.; Frota-Pessoa, S.; Frankel, R. B.; Holm, R. H. *Inorg. Chem.* **1982**, *21*, 1723−1728.
(50) Jordanov, J.; Roth, E. K. H.; Fries, P. H.; Noodleman, L. *Inorg. Chem.* **1990**, *29*, 4288−4292.
(51) Girerd, J.-J. *J. Chem. Phys.* **1983**, *79*, 1766−1775.

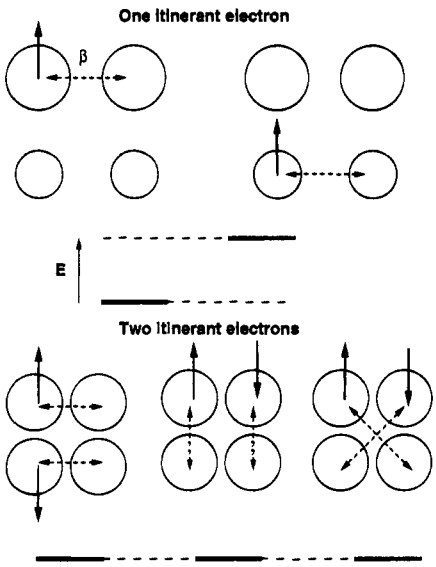

Figure 10. (Top) Illustration of the PKS mechanism for trapping of a single itinerant electron in a tetranuclear system in a delocalized pair. Theoretical studies[1] have revealed that symmetry breaking provides a ground state in which the itinerant electron is delocalized (by transfer interaction, double exchange) over two equivalent sites possessing expanded coordination spheres (upper left). A state of higher energy results by delocalizing the itinerant electron over the pair with the contracted coordination spheres (upper right). The core spins, which play an essential role in the pair-trapping mechanism, are not indicated. (Bottom) Three possible ways of delocalizing two itinerant electrons over two pairs of sites in a tetranuclear system of T_d symmetry. The symmetric local (PKS) distortions at the four sites are identical because each site accommodates half of an itinerant electron charge. Hence, the degeneracy of the three delocalization modes is retained, and there is no symmetry breaking of the PKS type.

following symmetry argument. The relevant symmetrized PKS coordinate in a tetranuclear unit has t_2 symmetry.[1b] As was argued above, t_2 vibrations do not couple A_i and E states and are therefore ineffective in distorting the diamagnetic ground state of the $[Fe_4S_4]^{2+}$ cluster. Site trapping of the itinerant electrons according to the PKS mechanism would require pseudo-Jahn−Teller interactions with states that are separated from the ground state by energies $\geq|\beta_0/5|$. In the previous work it was shown that the pair delocalization of a single itinerant electron in 3-Fe and 4-Fe clusters is found in the regime of predominant resonance interaction,[1] whereas in the present case the PKS mechanism is inactivated by strong resonance interaction. In order to attain pair diffentiation, one needs to introduce mechanisms which consider the structure dependence of *inter*site interactions, such as the mechanism studied here. We note in passing that the vibronic β-coupling mechanism as applied to the $d^5-d^5-d^6$ model for reduced Fe_4S_4 clusters is also capable of trapping the itinerant electron in a delocalized pair of Fe sites.[52]

Interpretation of r_{ij}. The transfer parameters, β_{ij}, may, in principle, depend on all structure variables of the Fe−S cluster. A general treatment of the structure dependence of β_{ij} would, however, require the introduction of an unwieldy number of unknown vibronic coupling constants. In order to simplify matters, we have assumed that the transfer parameters depend only on six structure parameters, Δr_{ij} (eq 6), describing the principal distortions relevant to the pair of Fe sites (i,j). We shall now attempt to assign a more definite meaning to the r_{ij} parameters.

A detailed account of the structures of the $[Fe_4S_4]^{2+}$ clusters in a series of synthetic analogs has been given by Holm and co-workers.[10-13] The distortion patterns of the 2+ clusters appear to be quite uniform. All closely approach idealized D_{2d} symmetry owing to a compression along a $\bar{4}$ symmetry axis; this results in eight long intralayer and four shorter interlayer Fe−S bonds.[53,54] The remaining structure parameters exhibit a more random behavior. For example, the difference of intra- and interlayer Fe−Fe distances ranges from −0.016 to 0.044 Å.[10] Taking into consideration the possibility of electron transfer mediated by sulfides, one might suspect the Fe−S−Fe bond angle to be an important structural determinant of β. However, the intra- and interlayer Fe−S−Fe bond angles obtained for the series-averaged structure differ only by 0.35°. The values for the angles $Cl-Fe_X-S_1$ and $Cl-Fe_X-S_2$, where S_1 is in the same layer as Fe_X and S_2 in the other layer, differ by about 6° in the analog with terminal chlorides. The corresponding differences in the cluster with SCH_2Ph side chains are, however, positive or negative depending on the Fe site considered and have a site-averaged value of 1°. Summing up, a plausible interpretation would be to identify the r_{ij} with the mean Fe−S bond distance, $(Fe-S)_{ij,av}$, taken over the Fe_2S_2 rhomb defined by the Fe sites i and j. Such an interpretation raises, however, an intriguing question concerning the orbital mechanism underlying the vibronic coupling defined in eq 6: On the one hand, the X-ray data show that the intralayer Fe−S distances are *longer* than the interlayer Fe−S distances. On the other hand, our theory indicates that the value of $|\beta_{intra}|$ should be *larger* than $|\beta_{inter}|$. Hence, the sign of Λ in eq 6 must be chosen such that an *increase* in $r_{ij} \sim (Fe-S)_{ij,av}$ results in an *enhancement* of the magnitude of β_{ij}, i.e., the sign of the distance dependence of β_{ij} is opposite to that expected on the basis of simple orbital overlap arguments. A similar problem is encountered in the interpretation of the computational results of Aizman and Case.[48] In order to match the C_{2v} symmetry of the broken-spin states to the D_{2d} symmetry of the structure, these authors arbitrarily assign the delocalized pairs to the two layers defined by the long Fe−S distances, despite the fact that stronger resonance may be obtained by delocalization over the shorter interlayer bridges. The contrary behavior may be explained by assuming that the distortions at the Fe sites (two long and one shorter Fe−S distances) stabilize oblate itinerant-electron orbitals lying in the layers defined by the long Fe−S distances, such that intralayer resonance is facilitated.[55] This consideration calls for a theoretical study of distortion effects on the iron orbital structure in the future.

Theoretical Model for $[Fe_4S_4]^{2+}-S_{cys}-Fe^{3+}$(heme)

In this section, we present a model for the description of the magnetic properties induced in the diamagnetic, broken-symmetry ground state of the $[Fe_4S_4]^{2+}$ cluster by an exchange coupling between one of the cubane iron sites and a high-spin ferric heme.

Electronic States. The oxidation states of the cluster and the heme are retained in the composite system $[Fe_4S_4]^{2+}-S_{cys}-Fe^{3+}$(heme) (see Introduction). The Mössbauer data of SiR^0 have shown that the magnetic hyperfine interactions and the isomer shift of the ferric siroheme are the same as those

(52) Bominaar, E. L. Unpublished results.

(53) Structures of a number of synthetic cubanes with "mixed" terminal ligands have been reported by D. Coucouvanis and co-workers.[54] Interestingly, these clusters possess $[Fe_4S_4]^{2+}$ cores with *non*-compressed D_{2d} idealized geometries. Although the idealized core symmetry is in agreement with our theoretical results, these systems are less appropriate for testing the present theory since the lowering of the cluster symmetry can be due to either an *intrinsic* (pseudo) Jahn−Teller effect or to the *"external"* effect of the mixed ligand environment.

(54) Kanatzidis, M. G.; Baenziger, N. C.; Coucouvanis, D.; Simopoulos, A.; Kostikas, A. *J. Am. Chem. Soc.* **1984**, *106*, 4500−4511.

(55) See, e.g., plate 1 of ref 43.

observed for a monomeric heme. Thus, we can assume here that the itinerant electrons (holes) are strictly confined to the cubane moiety. An appropriate basis of spin states for the composite system can be defined by coupling the basis states for the cube given in eq 1 to the spin $S_H = 5/2$ of the ferric high-spin heme

$$|(\alpha S_{cube}, S_H)S\rangle \tag{14}$$

in which α labels both the valence states and the subspins of the cube. Equation 14 will be referred to as the "cube-coupled" basis.

Our analysis is based on the plausible premise that the heme–cluster coupling does not affect the solutions for β_{intra} and β_{inter} of the vibronic coupling problem in the cube.[1d] The transfer interactions (double exchange within the cube) are then described by the operator H'_t in which the transfer parameters at the minima are unaffected by the heme–cluster coupling. Because we consider a fixed distortion, the elastic energies can be ignored (see above). In the cube-coupled representation, the Hamiltonian matrix for the operator $H'_t + H_{HDVV}$ can be evaluated as outlined in the section on $[Fe_4S_4]^{2+}$.

We shall make the plausible assumption that the weak exchange coupling between the heme spin, $S_H = 5/2$, and site Fe_D of the $[Fe_4S_4]^{2+}$cluster leads to a ground state with total spin $S = 5/2$ as observed by the EPR study of SiR[0].[21] The $S = 5/2$ space is spanned by the basis states given in eq 14 with S_{cube} ranging from 0 to 5, according to the common triangular condition. Both the reported low D value (6 cm^{-1}) and the g value ($g_\perp \approx 6$)[20] indicate that the local spin quartet states of the siroheme moiety lie a few thousand wavenumbers above the ground state,[56] such that we feel confident to describe the heme as a pure $S_H = 5/2$ manifold. The dimension of the $S = 5/2$ space, obtained by including the dimensions for the cubane states with $S_{cube} = 0$, 1, 2, 3, 4, and 5 given in Table 1, is 540. In the absence of heme–cube interaction, the energies of the system follow from diagonalization of the Hamiltonian matrix of $H'_t + H_{HDVV}$. For this case, the set of 540 eigenvalues is identical to the ensemble of eigenvalues for $S_{cube} = 0$, 1, 2, 3, 4, and 5 calculated for the isolated cube, using the same set of interaction parameters. The eigenvalues thus obtained for $\beta_{intra} = \beta_{inter} = 1$ and $J_{22} = J_{23} = J_{33} = 0$ are tabulated in the first six rows of Table 1.

HDVV Coupling to the Heme. The HDVV operator describing the exchange interaction of site D and the heme iron is defined as

$$H^{heme}_{HDVV} = [n_D J_{H3} + (1 - n_D)J_{H2}]\vec{S}_D \cdot \vec{S}_H \tag{15}$$

This definition allows for exchange-coupling constants of different strength depending on the valence state of Fe_D; the constants are denoted by J_{H3} for a ferric site and by J_{H2} for a ferrous site. Again, n_D keeps track of the itinerant hole. In order to cover a broad range of heme–cluster coupling constants, a non-perturbative diagonalization treatment of the total Hamiltonian, $H'_t + H_{HDVV} + H^{heme}_{HDVV}$, is adopted. H^{heme}_{HDVV} is diagonal in the "heme-coupled" basis which is defined as

$$|(((S_i,S_j)S_{ij},S^0_k)S_{ijk},(S^0_D,S_H)S^0_{DH})S\rangle$$
$$|(((S^0_i,S^0_j)S^0_{ij},S_k)S_{ijk},(S_D,S_H)S_{DH})S\rangle \tag{16}$$

where $\{i, j, k\} = \{A, B, C\}$, $\{C, A, B\}$, and $\{B, C, A\}$. The matrix elements are evaluated as

$$\langle(\alpha S_{ABC}, S^0_{DH})S|H^{heme}_{HDVV}|(\alpha' S_{ABC}', S^0_{DH}')S'\rangle = \delta_{S,S'}\delta_{\alpha,\alpha'}\delta_{S_{ABC},S_{ABC}'}\delta_{S^0_{DH},S^0_{DH}'}J_{H2}\{S^0_{DH}(S^0_{DH}+1) - S^0_D(S^0_D+1) - S_H(S_H+1)\} \tag{17a}$$

$$\langle(\alpha S_{ABC}, S_{DH})S|H^{heme}_{HDVV}|(\alpha' S_{ABC}', S_{DH}')S'\rangle = \delta_{S,S'}\delta_{\alpha,\alpha'}\delta_{S_{ABC},S_{ABC}'}\delta_{S_{DH},S_{DH}'}J_{H3}\{S_{DH}(S_{DH}+1) - S_D(S_D+1) - S_H(S_H+1)\} \tag{17b}$$

in which α labels the valence states and subspins occurring in eq 16. The diagonal matrix has been transformed to the cube-coupled representation by using the unitary matrices connecting the heme-coupled and cube-coupled bases and the resulting matrix was then added to the Hamiltonian matrix for the intra-cube interactions.

Results for $[Fe_4S_4]^{2+}$–S_{cys}–Fe^{3+}(heme)

The internal fields at the ^{57}Fe nuclei of the $[Fe_4S_4]^{2+}$ cluster determined by Mössbauer and ENDOR spectroscopy have provided solid evidence for the heme–cluster coupling in SiR and have given insight into the spin state of the $[Fe_4S_4]^{2+}$ cluster.[17–21,25] Being the only observables available for this purpose to date, the effect of the heme–cluster coupling on spin state is analyzed on the basis of the internal fields at the Fe sites. The internal field at cubane iron site X (=A, B, C, D) is described by the operator

$$\vec{H}^X_{int} = -\frac{[a_3 n_X + a_2(1 - n_X)]\vec{S}_X}{g_N \mu_N} \tag{18}$$

a_3 and a_2 denote intrinsic a-values for a ferric ($n_X = 1$) and a ferrous ($n_X = 0$) site, respectively, g_N the g factor, and μ_N the magneton of an ^{57}Fe nucleus. For convenience, the a_i-tensors are considered to be isotropic.[57,58] The internal fields can be expressed by means of the common effective A-tensor formalism. The details of calculation of the resulting A^X values, X = A, B, C, and D, are given in the Appendix.

A^X Values for $\beta_0 > 0$. Figures 11 and 12 show calculated A^X values for the cluster sites X = A, B, C, and D plotted as a function of the heme–cluster coupling parameter J_H for the cases $\beta_0 > 0$ and $\beta_0 < 0$, respectively. Within the accuracy of the present approach, it is reasonable to use the same a-values

(56) (a) Maltempo, M. M.; Moss, T. H. *Q. Rev. Biophys.* **1976**, *9*, 181–215. (b) Palmer, G. In *Iron Porphyrins*; Lever, A. B. P., Gray, H., Eds.; Addison-Wesley Publishing Co.: London, 1983; Part II, pp 43–88. (c) Bominaar, E. L.; Ding, X.-Q.; Gismelseed, A.; Bill, E.; Winkler, H.; Trautwein, A. X.; Nasri, H.; Fischer, J.; Weiss, R. *Inorg. Chem.* **1992**, *31*, 1845–1854.

(57) For the evaluation of spin-coupling models one generally uses the isotropic parts of the magnetic hyperfine tensors.[3] The **a**-tensors of high-spin Fe^{III} sites are generally isotropic, and studies of FeS_4 containing proteins and model compounds suggest a choice of $a_3 = a(Fe^{III}) = -20$ MHz; for details see ref 3. In addition to the isotropic contribution of the Fermi contact term, the **a**-tensors of high-spin Fe^{II} sites contain sizable orbital and spin-dipolar contributions. Since the spin-dipolar contribution is traceless, it will not contribute to the quantity $a_{av} = (a_x + a_y + a_z)/3$. The orbital contribution to the **a**-tensor is proportional to $(g_i - 2)$ where the g_i are the principal components of the g-tensor; for $Fe^{II}S_4$ sites, the anisotropy of the g-tensor is generally $\leq 10\%$. For $Fe^{II}S_4$ complexes and $[Fe_2S_2]^{1+}$ clusters one can estimate the orbital contribution from the observed zero-field splittings and g-values, respectively.[58] We have argued previously[3] that $a_{av}(Fe^{II}) = a_2 \approx -22$ MHz for $Fe^{II}S_4$ sites. Since a_2 and a_3 differ by just 10%, we have chosen here $a_3 = a_2 = -21$ MHz. Hence, our main result $A^A = A^B \approx -A^C \approx -A^D$ would still hold if one uses different a-values for the ferric and ferrous sites.

(58) Trautwein, A. X.; Bill, E.; Bominaar, E. L.; Winkler, H. *Structure and Bonding*; Springer: Berlin, Heidelberg, 1991; Vol. 78, pp 1–95.

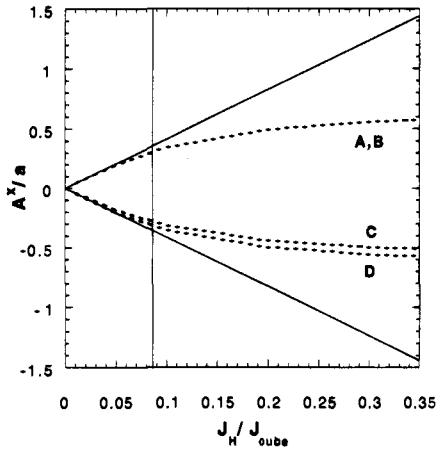

Figure 11. Magnetic hyperfine parameters, A^X, calculated with the theoretical model for the system $[Fe_4S_4]^{2+}-S_{cys}-Fe^{3+}$(heme) at the cubane sites X (=A, B, C, D) indicated in the figure, as a function of the coupling constant, J_H, for the exchange interaction between site Fe_D of the $[Fe_4S_4]^{2+}$ cluster for positive β_0 (broken curve). A^X is expressed in units of the intrinsic a-value of cubane iron; for simplicity it is assumed that the a-values are independent of the site and the oxidation state, $a_2 = a_3 = a$.[57] J_H is given in units of J_{cube}, the effective coupling constant for interlayer exchange in the cube. The vertical line marks the value of J_H for which the calculated A^X values match the experimental data in the $S = 5/2$ state of SiR^0. The two solid lines that are tangent to the exact curves depict the approximate relationship given in eq 23. Parameters used: $\beta_{intra} = 4000\ cm^{-1}$, $\beta_{inter} = 3600\ cm^{-1}$, $J_{22} = 80\ cm^{-1}$, $J_{23} = 160\ cm^{-1}$, and $J_{33} = 360\ cm^{-1}$. J_{cube} is taken as the average of the latter three values, $200\ cm^{-1}$.

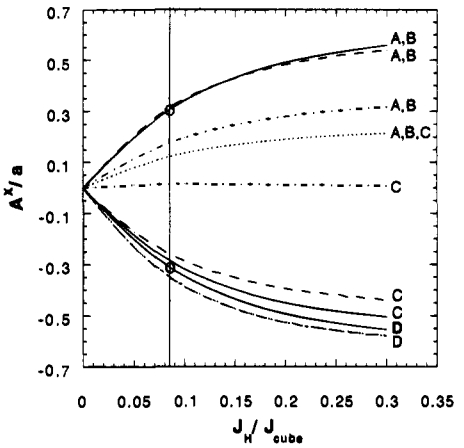

Figure 12. Magnetic hyperfine parameters, A^X, calculated with the theoretical model for the system $[Fe_4S_4]^{2+}-S_{cys}-Fe^{3+}$(heme) at the cubane sites X (=A, B, C, and D) indicated in the figure, as a function of the coupling constant, J_H, for the exchange interaction between the heme iron site D of the $[Fe_4S_4]$ moiety for a number of negative β_0 values: $\beta_{inter} = -2000\ cm^{-1}$ ($\beta_{inter}/\beta_{intra} = 0.500$, −), $-3960\ cm^{-1}$ (0.99, − −), $-3996\ cm^{-1}$ (0.999, −·−), and $-4000\ cm^{-1}$ (1.000, ···). For the latter three cases, the values for A^D almost coincide (− ·· −). A^X is expressed in units of the intrinsic a-value of cubane iron, which is assumed to be independent of the site and the oxidation state, $a_2 = a_3 = a$.[57] J_H is given in units of J_{cube}, the effective coupling constant for interlayer exchange in the cube. The vertical line marks the value of J_H for which the calculated A^X values match the experimental data (○) for the $S = 5/2$ state of SiR^0. Parameters used: $\beta_{intra} = -4000\ cm^{-1}$, $J_{22} = 80\ cm^{-1}$, $J_{23} = 160\ cm^{-1}$, and $J_{33} = 360\ cm^{-1}$.

for all cluster Fe sites regardless of the oxidation state,[57] i.e. we take $a_2 = a_3 \equiv a$; this allows us to express the A^X values conveniently in units of a. Our results show that weak heme−cluster coupling can already produce A^X values of the same magnitude as observed in oxidized sulfite reductase. The theory presented above predicts that the symmetry of an isolated ($J_H = 0$) $[Fe_4S_4]^{2+}$ cluster is lowered from T_d to D_{2d}. In the broken-symmetry states, the Fe sites are arranged in delocalized pairs, (A,B) and (C,D), which are locked-in by resonance parameters of different strength, $|\beta_{inter}| < |\beta_{intra}|$. It can be seen from Figures 11 and 12 that evidence for delocalized pairs is expressed in the A^X values which exhibit the pair pattern $A^A = A^B \approx -A^C \approx -A^D$. The observation of pairwise equivalent A^X values is not surprising even if one considers that Fe_D is distinguished by the coupling to the heme. This observation reflects the internal electronic structure of the $[Fe_4S_4]^{2+}$ cluster. Thus, the coupling of the heme to Fe_D perturbs the internal spin coupling of the cluster, leading to first-order mixing of an $S_{cube} = 1$ state into the ground state (see below). Because the spins of Fe_D and Fe_C are parallel aligned by the strong double-exchange interactions, the changes at Fe_D are transmitted to Fe_C. Since the (C,D) pair has, in turn, strong antiferromagnetic interactions with (A,B), the local spins at Fe_A and Fe_B are oriented opposite to those of Fe_C and Fe_D. Since the signs and the magnitudes of the internal magnetic fields reflect the expectation values of the local spins, we obtain the A^X value patterns of Figures 11 and 12. Pair patterns are obtained nearly over the entire range of $\beta_{inter}/\beta_{intra}$ ratios: for $0 < \beta_{inter}/\beta_{intra} < 0.99$, $A^A = A^B$ changes only by 1.5% whereas A^C and A^D vary by 6% and 3%, respectively.[59] In the limit of vanishing vibronic interactions, i.e. $\beta_{inter}/\beta_{intra} = 1$, the symmetry of the effective Hamiltonian changes to C_{3v} and the pattern of A^X values goes over into $A^A = A^B = A^C \approx -A^D/3$;[60] this limit involves degenerate states (see Figures 5 and 6) and does not seem to be of practical interest to the SiR^0 problem. (A treatment of this limit would also require consideration of state mixing by the local zero-field splittings.)

The ground state that exhibits the pattern $A^A = A^B \approx -A^C \approx -A^D$ is primarily a linear combination of the following two configurations

$$|0\rangle \equiv \left|\frac{5}{2},\left(\frac{9}{2},\frac{9}{2}\right)0;\frac{5}{2}\right\rangle \tag{19a}$$

$$|1\rangle = \left|\frac{5}{2},\left(\frac{9}{2},\frac{9}{2}\right)1;\frac{5}{2}\right\rangle \tag{19b}$$

with the nomenclature $|S_H,(S_{CD},S_{AB})S_{cube};S\rangle$. The major component, $|0\rangle$, follows from the diamagnetic, pair-delocalized, broken-symmetry ground state of the cube by spin coupling to S_H. The minor component, $|1\rangle$, is mixed into the ground state by the heme coupling; it derives from the first-excited, pair-delocalized state with $S_{cube} = 1$ and confers paramagnetic character to *all* Fe sites of the cluster. As is shown in Figures 5 and 6, the $S_{cube} = 1$ state is separated from the ground state by an energy gap $\Delta E = J_{cube}$ throughout the relevant β-ratio range. The indistinguishability between the sites in each of the pairs (A,B) and (C,D) is strictly retained under the admixture

(59) For $\beta_{inter} \neq \beta_{intra}$ and $J_H \neq 0$, the symmetry of the composite Hamiltonian, $H'_1 + H_{HDVV} + H^{heme}_{HDVV}$, is C_{2v}, such that the sites A and B are equivalent: $A^A = A^B$. The percent changes mentioned in the text are obtained for $J_H = 20\ cm^{-1}$ and the cubane parameters used in Figure 6.

(60) This property only becomes apparent by averaging the A^X values over the two components of the E ground state for $\beta_0 > 0$ (Figure 6). The pattern $A^A = A^B \approx -A^C \approx -A^D$ is retained even in the close proximity of $\beta_{inter}/\beta_{intra} = 1$, since the six total-spin states obtained by composing the heme spin with the diamagnetic ground levels of the cubane transfer operator do not interact through the heme−cluster exchange-coupling operator. Adopting the exchange-coupling constants used in Figure 6, an $A^A = A^B \approx A^C \approx -A^D/3$ type of pattern is only found for $\beta_{inter}/\beta_{intra} > 0.9995$. In the limiting case, the C_{3v} symmetry can be considered as a subgroup of the T_d symmetry of the Hamiltonian for the cubane moiety. As $E(T_d)$ states correlate to $E(C_{3v})$ states, the degeneracies in the level scheme of the six diamagnetic states shown in Figure 6 are retained under the heme coupling.

of $|0\rangle$ and $|1\rangle$. Mutually, however, the two pairs differ due to the heme−cluster coupling.

In order to derive an analytical expression for the dependence of the A^X values, the heme-induced interaction between the broken-symmetry eigenstates, $|0\rangle$ and $|1\rangle$, of the Fe−S cluster Hamiltonian is treated in perturbation theory. In first order, the ground state can be written as

$$|\psi\rangle \approx |0\rangle - \frac{J_H}{J_{cube}}\langle 1|\vec{S}_H\cdot\vec{S}_D|0\rangle|1\rangle \qquad (20)$$

The composition of the ground state suggests that the five-spin coupling problem can be effectively reformulated as a three-spin problem, involving S_{AB}, S_{CD}, and S_H. The indistinguishability of sites C and D in states $|0\rangle$ and $|1\rangle$ implies that

$$\langle 1|\vec{S}_H\cdot\vec{S}_D|0\rangle = \frac{1}{2}\langle 1|\vec{S}_H\cdot\vec{S}_{CD}|0\rangle \qquad (21)$$

in which the matrix element involving the local spin, $\vec{S}_D$, is replaced by half of the matrix element involving the pair spin $\vec{S}_{CD} = \vec{S}_C + \vec{S}_D$. Similarly, the A^X values are expressed as

$$\frac{A^X}{a} \approx \frac{1}{2M}\langle\psi;M|S_{XY,z}|\psi;M\rangle \qquad (22)$$

with (X,Y) forming one of the pairs, (A,B) or (C,D); the approximately equal sign indicates that the expressions in eqs 20 and 22 are evaluated by the perturbation treatment. Substitution of eqs 20 and 21 into eq 22 yields, in linear approximation, the expression for the A^X which is given in eq 23. The matrix element can be evaluated by straightforward application of spin-coupling techniques.

$$\frac{A^A}{a} = \frac{A^B}{a} \approx -\frac{A^C}{a} \approx -\frac{A^D}{a} \approx \frac{2}{35}\frac{J_H}{J_{cube}}\langle 1|\vec{S}_H\cdot\vec{S}_{CD}|0\rangle^2 \approx 4.1\frac{J_H}{J_{cube}} \qquad (23)$$

It is seen that the ratio of the observable and the intrinsic magnetic hyperfine parameters is proportional to J_H/J_{cube}. The former ratio is about 0.3 in the $S = 5/2$ state of SiR^0,[21] implying that only a weak heme coupling, $J_H = 0.07J_{cube} \approx 15$ cm^{-1} for $J_{cube} \approx 200$ cm^{-1}, is needed to generate the observed internal fields. A sign reversal of J_H leads to a simultaneous sign flip of all the A^X values. The sign of J_H in SiR^0 cannot be deduced from any of the experimental data available to date, as such a determination would require the structural assignment of the spectroscopically discernable sites. A^A/a and A^B/a are positive for antiferromagnetic heme coupling ($J_H > 0$). The signs of the A^X/a values can be understood from a pictural representation of the ground state: $\vec{S}_{AB}$ is antiparallel aligned with respect to $\vec{S}_{CD}$ by strong antiferromagnetic exchange. Depending on the sign of J_H, $\vec{S}_{AB}$ is either parallel or antiparallel aligned relative to the "majority" spin $\vec{S}_H$. The spin of the heme iron provides the frame of reference in a Mössbauer experiment because the coupled spin assembly is aligned by interaction of the applied field with the (dominant) magnetic moment of the heme iron.

The range of validity of the linear expression for A^X/a versus J_H/J_{cube} given in eq 23 is evident from inspection of Figure 11. It can be seen that the approximate expression gives an excellent description of the exact results for $J_H/J_{cube} < 0.05$. For stronger heme−cluster couplings, however, the A^X gradually saturate for $J_H/J_{cube} > 0.3$. The vertical line drawn just beyond the limit of the linear regime marks the J_H/J_{cube} ratio where the exact results match the experimental data for the A^X values in the $S = 5/2$ state in SiR^0. The J_H value thus obtained implies a slightly stronger heme−cluster coupling constant (17 cm^{-1} for $J_{cube} =$ 200 cm^{-1}) than the value deduced from the linear model (eq 23). The calculations predict small differences (≈0.3 MHz) between A^C and A^D. While this difference falls within the margins of experimental uncertainties, one should keep in mind that it may be either amplified or attenuated by neglected anisotropies or differences caused by structural inequivalence of the sites (such as differences in cysteinyl bonding, for instance).

Finally, evaluation of the A value of the heme iron, A^H, with eq 20, leads, in second-order, to the expression

$$A^H = \left[1 - 8.25\left\{\frac{J_H}{J_{cube}}\right\}^2\right]a_H \qquad (24)$$

where a_H is the a-value of the uncoupled Fe^{III}-siroheme. Using $J_H/J_{cube} = 0.07$ yields $A^H \approx 0.96a_H$,[61] which shows that the heme−cluster coupling perturbs the heme iron only in a minor way. A^H thus cannot be used to determine J_H, in the absence of a suitable reference compound with $J_H = 0$.

A^X Values for $\beta_0 < 0$. Figure 12 shows a plot of A^X values versus J_H/J_{cube} for different values of the ratio $\beta_{inter}/\beta_{intra}$ in which both the numerator and the denominator are negative. Comparison with Figure 11 shows that the plots of the A^X values obtained for $\beta_0 < 0$ and $\beta_0 > 0$ have similar features. For instance, the A^X values plotted in Figure 12 conform to the pattern $A^A = A^B \approx -A^C \approx -A^D$ for $\beta_{inter}/\beta_{intra} < 0.99$. Moreover, the relationship between A^X/a and J^H/J_{cube} is almost linear for $J_H/J_{cube} < 0.05$ and the slope is nearly equal to that obtained for $\beta_0 > 0$ in the same J_H/J_{cube} range. As a consequence, the value A^X/a (≈0.3) obtained for SiR^0 gives the same value for the heme−cluster coupling constant, $J_H \approx \pm 17$ cm^{-1}, in both the positive and negative β_0 range. As can be seen from Figure 12, there is a smooth transition as a function of the β-ratio between the patterns $A^A = A^B \approx -A^C \approx -A^D$ (C_{2v}) and $A^A = A^B = A^C \approx -A^D/3$ (C_{3v}), as expected for a nondegenerate ground state.

Conclusions

The main conclusions of the analysis of the theoretical model for the $[Fe_4S_4]^{2+}$ cluster are as follows:

(1) The electron-transfer operator for the tetranuclear system $d^5-d^5-d^6-d^6$ of T_d symmetry with paramagnetic high-spin cores containing two itinerant electrons has a degenerate ground manifold, comprising states with different spin and orbital character, for both positive and negative values of the transfer parameter, β_0 (the sign of β_0 refers to the equivalent hole picture, $d^5-d^5-d^4-d^4$).

(2) The vibronic coupling due to the structure dependence of the transfer parameters, $\beta_{ij} = \beta_0 + \Lambda\Delta r_{ij}$, gives rise to Jahn−Teller distortion from T_d to D_{2d} symmetry. This result is independent of the sign of β_0 and is in agreement with the distortions observed in the X-ray structure of $[Fe_4S_4]^{2+}$ cores in proteins and model complexes with identical terminal ligands, indicating that the D_{2d} symmetry is an *intrinsic* property of the cluster rather than a feature imposed by the environment.

(3) The broken-symmetry ground state obtained for $\beta_0 > 0$ reflects two layers, each containing a delocalized itinerant electron. The spin of the each layer is 9/2. Owing to interlayer resonance, the ground state for $\beta_0 < 0$ has a more complex composition than that obtained for $\beta_0 > 0$. Despite the greater complexity, the principal component of the ground state for $\beta_0 < 0$ can still be recognized as resulting from interaction of two delocalized 9/2 layers.

(61) Full calculations yield factors >0.96.

(4) The broken-symmetry ground state of the tetranuclear cluster is diamagnetic in the presence of antiferromagnetic HDVV exchange. The first-excited paramagnetic state has spin $S_{cube} = 1$. The energy gap between the two states is mainly determined by an effective coupling constant for interlayer exchange.

The conclusions of the analysis for the $[Fe_4S_4]^{2+}-S_{cys}-Fe^{3+}$-(heme) assembly can be formulated as follows:

(5) Weak exchange coupling (J_H) of one of the cubane sites, Fe_D, to a high-spin Fe^{3+} generates weak magnetic hyperfine fields at all iron sites of the $[Fe_4S_4]^{2+}$ cluster. The fields are mainly induced by admixture of the first-excited spin triplet, $S_{cube} = 1$, into the diamagnetic broken-symmetry ground state.

(6) The calculated A^X values appear as $A^A = A^B \approx -A^C \approx -A^D$ over a broad range of parameter values that extends to the proximity of the weak vibronic-coupling limit, $\beta_{inter}/\beta_{intra} < 0.99$. The pattern obtained over this range matches the pattern observed in Mössbauer studies of the $S = 5/2$ state of SiR^0.

(7) There exists, in good approximation, a linear relationship between A^X/a and J_H/J_{cube}, provided that the latter ratio is smaller than 0.05.

(8) In the framework of the theoretical model presented here, the interpretation of the ^{57}Fe A^X values in the $S = 5/2$ state of SiR^0 requires a heme−cluster coupling constant, $J_H = \pm 17$ cm^{-1}. The sign of J_H is, however, indeterminate.

Acknowledgment. This research was supported by the National Institutes of Health Grant GM22701 and the National Science Foundation Grant MCB-9406224 to E. M.

Appendix

According to the Wigner−Eckart theorem for vector operators, the matrix elements of the internal-field operator (eq 18) in a $(2S + 1)$-dimensional spin multplet, $|\psi S;M\rangle$, can be expressed as a product of a global A value and a matrix element of the total spin operator:[62]

$$-g_N\mu_N\langle\psi S;M|\vec{H}^X_{int}|\psi S;M'\rangle = A^X_\psi\langle S;M|\vec{S}|S;M'\rangle \quad (A.1)$$

in which the magnetic quantum numbers defined by S_z are denoted as M and M'. The states, $|\psi S\rangle$, considered here are eigenstates of the total Hamiltonian $H'_t + H_{HDVV} + H^{heme}_{HDVV}$. The superscripts and subscripts of the A value indicate that this quantity is dependent on both the site and the eigenstate. The A^X_ψ value can be evaluated as follows. We define a new "A-site coupled" basis in which the spin of site A is coupled to the resultant spin of the remaining sites

$$|(S_A((S_i(S^0_j,S^0_k)S^0_{jk})S_{ijk},S_H)S_{ijkH})S\rangle$$
$$|(S^0_A((S_i,S_j)S_{ij},S^0_k)S_{ijk},S_H)S_{ijkH})S\rangle \quad (A.2)$$

where the ferrous sites are denoted by the superscript zero, and $\{i, j, k\} = \{B, C, D\}$, $\{C, D, B\}$, and $\{D, B, C\}$. H^A_{int} is diagonal with respect to the subspin- and valence-state labels

$$\langle(S^\alpha_A,\alpha S_{BCDH})S;M|\vec{H}^A_{int}|S^{\alpha'}_A,\alpha' S_{BCDH}')S;M'\rangle = \delta_{\alpha,\alpha'}\delta_{S_{BCDH},S_{BCDH}'}a_\alpha \frac{S^\alpha_A(S^\alpha_A+1) - S_{BCDH}(S_{BCDH}+1) + S(S+1)}{2S(S+1)} \langle S;M|\vec{S}|S;M'\rangle \quad (A.3)$$

All subspin and valence labels that are not explicitely listed in eq A.3 are lumped into label α. Furthermore, we have adopted the notation $a_\alpha = a_2$ and $S^\alpha_A = S^0_A$ if site A is ferrous, and $a_\alpha = a_3$ and $S^\alpha_A = S_A$ if site A is ferric. The eigenvectors of the total Hamiltonian, which have been evaluated in cube-coupled representation (see above), are converted to the A-site coupled representation by unitary transformation, leading to the expansion

$$|\psi S\rangle = \sum_{\alpha,S_{BCDH}}^{540} c_{\alpha,S_{BCDH}}|(S^\alpha_A,\alpha S_{BCDH})S\rangle \quad (A.4)$$

The A values can be written as in the first line of eq A.5 by using the defining eq A.1 and can then be expressed as a probability-weighted summation over the matrix elements given in eq A.3 (second line of eq A.5).

$$A^A_\psi = \frac{1}{\langle S;M|S_z|S;M\rangle}\langle\psi S;M|H^A_{int,z}|\psi S;M\rangle = \frac{1}{M}\sum_{\alpha,S_{BCDH}}^{540} c^2_{\alpha,BCDH}\langle(S^\alpha_A,\alpha S_{BCDH})S;M|H^A_{int,z}|(S^\alpha_A,\alpha S_{BCDH})S;M\rangle \quad (A.5)$$

A similar procedure has been applied to the calculation of the A^X_ψ values of the sites B, C, and D.

JA950599G

(62) Brink, D. M.; Satchler, G. R. *Angular Momentum*; Oxford Library of Physical Sciences: Clarendon, Oxford, 1968.